

Stochastic modeling of superfluorescence in compact systems

Stasis Chuchurka* and Vladislav Sukharnikov

*Deutsches Elektronen-Synchrotron DESY, Hamburg 22607, Germany
Department of Physics, Universität Hamburg, Hamburg 22761, Germany*

Andrei Benediktovitch

Deutsches Elektronen-Synchrotron DESY, Hamburg 22607, Germany

Nina Rohringer†

*Deutsches Elektronen-Synchrotron DESY, Hamburg 22607, Germany
Department of Physics, Universität Hamburg, Hamburg 22761, Germany*

(Dated: December 12, 2023)

We propose an approach based on stochastic differential equations to describe superfluorescence in compact ensembles of multi-level emitters in the presence of various incoherent processes. This approach has a numerical complexity that does not depend on the number of emitters. The stochastic differential equations are derived directly from the quantum master equation. In this study, we present a series of numerical examples, comparing our solution to exact calculations and discussing the limits of applicability. For many relevant cases, the proposed stochastic differential equations provide accurate results and correctly capture quantum many-body correlation effects.

I. INTRODUCTION

Superfluorescence is a notable phenomenon in quantum optics, that is observed when incoherently excited atoms collectively emit radiation in the form of a highly energetic and short burst of light. The initially produced spontaneous emission couples the dipole moments of atoms, allowing them to synchronize the emission of photons. The phenomenon of superfluorescence traces its origins back to the seminal work of Dicke [1]. Since then, it has garnered significant theoretical interest [2–7] and has been a source of inspiration for numerous experimental studies. These studies include early demonstrations in gases [8–11] and solids [12], as well as more recent demonstrations in quantum dots [13], nitrogen-vacancy centers [14], cold atoms [15, 16], and nuclei [17]. Earlier investigations spanned from optical [11] and infrared [18, 19] to millimeter [20, 21] wavelengths. The recent emergence of X-ray free-electron lasers has provided exciting opportunities to observe the phenomenon of superfluorescence in the X-ray domain [22–26]. Nevertheless, these new opportunities bring additional complications to the theoretical description of the underlying phenomena. For example, X-ray transitions often undergo significant decoherence in the form of the Auger-Meitner effect, which can intensely compete with the excitation process and substantially disrupt the synchronization of atomic dipoles. Therefore, the theoretical models that previously proved efficient need thorough revision.

In Ref. [1], Dicke introduced a minimal model necessary for observing collective spontaneous emission. This model comprises a system of identical two-level quan-

tum emitters interacting with a quantized electromagnetic field assumed to be uniform across the ensemble. Being indistinguishable, N emitters evolve through a ladder of $(N+1)$ collective many-body states, synchronizing the radiation phases of the different emitters. This basic model can be generalized to include multi-level emitters [27] and incoherent processes [28, 29], which only partially diminish the collective nature of the interaction with the field. Providing invaluable insight from a theoretical point of view, these approaches, however, do not suggest an efficient strategy for numerical studies. Decomposing the quantum states in the basis set that accounts for the permutation symmetry results in a system of equations, the number of which grows polynomially with the number of atoms N . Although the resulting polynomial complexity allows treating a moderately large number of atoms ($N \lesssim 100$) with a relatively acceptable computational effort [28], the problems involving a realistically large number of atoms still remain challenging.

This numerical complexity has been acknowledged previously, as experiments often involve macroscopic numbers of atoms $N \gg 1$. As outlined in Ref. [4], when the system is instantaneously excited, and there are no competing incoherent processes, quantum effects dominate in the early stages of superfluorescence. Subsequently, the evolution becomes classical, and we can effectively simulate the dynamics of quantum emitters by solving Bloch equations with statistically distributed initial dipole moments. By considering multiple regions with independently distributed initial conditions, we can conduct a numerical analysis of macroscopic distributed systems.

However, if the initial incoherent excitation triggering superfluorescence is not instantaneous, and the quantum stage is further complicated by various incoherent processes, random initial conditions are no longer applicable. In such cases, several phenomenological strategies have been proposed. For instance, in Refs. [30–33], random

* stasis.chuchurka@desy.de

† nina.rohringer@desy.de

initial conditions have been replaced by phenomenological noise terms acting as source terms in the Maxwell-Bloch equations. Nevertheless, as these methods are not derived from first principles, they come with certain limitations. For example, the widely used methodology proposed in Ref. [31] produces an incorrect temporal profile of spontaneous emission, as highlighted in Refs. [34, 35].

In summary, there is currently no numerically efficient and sufficiently accurate methodology available for providing a reliable quantitative characterization of collective spontaneous emission involving an arbitrary number of multi-level emitters, especially in the presence of incoherent processes and excitation. Therefore, our objective is to establish such a formalism based on first principles. The development of this formalism draws inspiration from a many-body phase-space description utilizing the positive P function. (for more details and examples, see Refs. [36–40]). While this approach offers a direct path to stochastic equations that can be efficiently sampled in a Monte Carlo style, it, unfortunately, features certain limitations extensively discussed in Refs. [41–43]. The present article offers an in-depth analysis of how these limitations affect the simulation of superfluorescence.

Given the need to benchmark the proposed theoretical methodology, this article focuses exclusively on superfluorescence in compact systems. This choice is motivated by the fact that it can be exactly solved using methods based on the decomposition of the quantum state. Specifically, we adopt the methodology presented in Ref. [28]. The numerical benchmark suggests that the proposed methodology provides satisfactory results for a wide range of parameter values. Discrepancies, however, arise when the system evolves into a dark many-body state. Furthermore, we demonstrate that the presence of incoherent processes mitigates the prominence of this issue.

In our formalism, neither the form nor the number of equations depends on the number of emitters N in the system. N only enters the equations as a parameter, making the methodology free from the numerical difficulties inherent in techniques based on quantum state decomposition. For the extended methodology suitable for analyzing distributed systems, we refer the interested reader to Ref. [44].

Let us outline the structure of the article. In Sec. II, we construct the master equation for superfluorescence in compact systems. In Sec. III, we rephrase the quantum-mechanical problem in terms of stochastic differential equations. We also address numerical challenges encountered during the simulations and propose potential solutions. In Sec. IV, we analyze various conditions under which the phenomenon of superfluorescence can be observed. We begin with the simplest example in Sec. IV A, involving the cooperative emission of instantly excited two-level atoms. By comparing our simulations with those based on the methodology presented in Ref. [28], we evaluate the performance of our proposed method

for various numbers of atoms and initial conditions. We demonstrate that under specific circumstances when the system evolves into a dark many-body state, our methodology fails to reproduce the correct behavior. When the influence of such states is not significant, we achieve adequate results with minimal computational resources. In Sec. IV B, we explicitly include excitation via incoherent pumping. This accentuates the challenge posed by dark states. We will demonstrate how this issue can be mitigated by introducing decoherence typically present in experimental conditions. In Secs. IV C and IV D, we conclude the numerical examples by studying multi-level effects in superfluorescence observed in V - and Λ -systems. In this case, we demonstrate the performance of the methodology by constructing non-trivial three-particle correlation functions. In Sec. V, we give an overview of the applicability limits of our methodology and share empirical observations made during the numerical studies.

II. COMPACT SYSTEMS

The dynamics of the field in distributed systems is generally complex and depends on many factors that are insignificant for our goal to introduce the key ideas of our stochastic formalism applied to superfluorescence. In Ref. [1], it was supposed that in a compact ensemble of atoms, the system size was considerably smaller than the wavelength of the field. As a result, the atoms saw an identical field. This simplified model neglects the influence of dipole-dipole interactions between the atoms that was shown to be detrimental to observing superfluorescence [4, 45–47]. In certain cases of strong dipole-dipole interactions, the so-called dipole blockade [48], suppresses the electronic transitions initiated by a narrow-band field. The effects of dipole-dipole interactions strongly depend on the geometry and distances between the emitters, thus defining the minimal interatomic distance beyond which the superradiant behavior takes place [49, 50].

Numerical analysis with fully implemented dipole-dipole interactions is quite involved since it requires individual treatment of each atom due to the broken symmetry. One possible workaround is to replace the dipole-dipole interacting atoms with atoms that interact only through the radiative field but possess different transition frequencies, mimicking the impact of the dipole-dipole interactions [51]. Another approach is to reduce the effect of the dipole-dipole interactions by introducing a bad cavity or an elongated dilute atomic system. The former approach will ultimately lead us to superfluorescence in compact systems. As shown in Ref. [52], proper use of a cavity eliminates the effect of dipole-dipole interactions, which may explain a good agreement between experiments in Refs. [53, 54] and a simple Dicke model without any account of dipole-dipole interactions. Indeed, a cavity selects optical wave vectors close to the tran-

sition frequency ω_0 , which filters out the dipole-dipole interactions and simplifies the spatial dependence of the field. Based on these assumptions, the problem of superfluorescence is considerably simplified and reduces to a Dicke master equation that we aim to solve by means of stochastic differential equations.

Consider a system of N identical multi-level atoms characterized by a system of levels $\{|p\rangle\}$, energies $\hbar\omega_p$, and the following free Hamiltonian:

$$\hat{H}_0 = \sum_p \hbar\omega_p \sum_a \hat{\sigma}_{a,pp}.$$

Here, we utilize the operators $\hat{\sigma}_{a,pq} = |p\rangle_a \langle q|_a$ to describe transitions between states for each atom a . Initially, atoms are uncorrelated and described by a density matrix symmetric under any permutation.

The atomic levels are coupled to the quantized electric displacement field $\hat{\mathbf{D}}(\mathbf{r})$. The presence of the cavity makes its amplitude uniform across the sample. We suppose a field of single carrier wave vector \mathbf{k}_0 associated with the transition frequency $\omega_0 = ck_0$ given by

$$\begin{aligned} \hat{\mathbf{D}}(\mathbf{r}) &\approx \hat{\mathbf{D}}^{(+)} e^{i\mathbf{k}_0\mathbf{r}} + \hat{\mathbf{D}}^{(-)} e^{-i\mathbf{k}_0\mathbf{r}} \\ &= \sum_{\lambda} \left(D_0 \hat{a}_{\lambda} \mathbf{e}_{\lambda} e^{i\mathbf{k}_0\mathbf{r}} + D_0^* \hat{a}_{\lambda}^{\dagger} \mathbf{e}_{\lambda}^* e^{-i\mathbf{k}_0\mathbf{r}} \right). \end{aligned}$$

Here, $D_0 = i\sqrt{\hbar\omega_0\varepsilon_0/[2V]}$, V is the quantization volume, \hat{a}_{λ} and $\hat{a}_{\lambda}^{\dagger}$ are the bosonic field operators, and the vectors \mathbf{e}_{λ} are the polarizations of the field perpendicular to \mathbf{k}_0 . Among all the atomic levels, the light only couples two subsets: the ground state manifold $|g\rangle$ and the excited state manifold $|e\rangle$. Their energy splittings, denoted as $\omega_{ee'} = \omega_e - \omega_{e'}$ and $\omega_{gg'} = \omega_g - \omega_{g'}$, are assumed to be much smaller than the carrier frequency ω_0 . Later in this article, we use indices p, q, r, s, i, j to represent any arbitrary state, while specifically reserving indices g and e for states from the ground and excited state manifolds, respectively. The dynamics of the atomic populations is supposed to change on time scales large compared to $1/\omega_0$, so that non-resonant contributions are neglected. Based on these approximations, we write the following interaction Hamiltonian

$$\hat{V} = -\frac{1}{\varepsilon_0} \hat{\mathbf{D}}^{(+)} \sum_{e,g} \mathbf{d}_{eg} \sum_a \hat{\sigma}_{a,eg} e^{i\mathbf{k}_0\mathbf{r}_a} + \text{h.c.} \quad (1)$$

where \mathbf{d}_{pq} are the matrix elements of the dipole moment operators. The atomic coherences assemble in the sum $\sum_a \hat{\sigma}_{a,eg} e^{i\mathbf{k}_0\mathbf{r}_a}$ reflecting the collective interaction with the field mode¹. Henceforth, we omit the multiplier $e^{i\mathbf{k}_0\mathbf{r}_a}$ since it can be adjusted by shifting the phases of

the states $|e\rangle$ and $|g\rangle$. We introduce collective dipole moments $\hat{\mathbf{P}}^{(\pm)}$ composed of the phased operators $\hat{\sigma}_{a,pq}$ as follows:

$$\begin{aligned} \hat{\mathbf{P}}^{(-)} &= \sum_{eg} \mathbf{d}_{eg} \sum_a \hat{\sigma}_{a,eg}, \\ \hat{\mathbf{P}}^{(+)} &= \sum_{eg} \mathbf{d}_{ge} \sum_a \hat{\sigma}_{a,ge}. \end{aligned}$$

This gives a compact expression for the interaction Hamiltonian in Eq. (1):

$$\hat{V} = -\frac{1}{\varepsilon_0} \left(\hat{\mathbf{P}}^{(-)} \hat{\mathbf{D}}^{(+)} + \hat{\mathbf{P}}^{(+)} \hat{\mathbf{D}}^{(-)} \right). \quad (2)$$

Having only one mode in a cavity simplifies the spatial dynamics; however, it can only lead to optical phenomena such as quantum Rabi oscillations, collapse, and revivals [55, 56], which we do not intend to analyze in this article. Additionally, achieving collective spontaneous emission requires a substantial leakage of photons, as discussed in, for example, Ref. [5].

After an atom emits a photon, it makes effectively $Q/[k_0L]$ passes² through the cavity before it gets damped. Here, Q is the quality factor, and L is the length of the cavity. In order to have collective spontaneous emission, the dynamics of the atomic populations and coherences must be much slower than the leakage of the field. In these circumstances, we can trace out the field degrees of freedom by applying the Born-Markov approximation, which leads to the well-known Dicke master equation formulated for multi-level atoms

$$\begin{aligned} \frac{d\hat{\rho}(t)}{dt} &= \mathcal{L}[\hat{\rho}(t)] = \frac{i}{\hbar} \left[\hat{\rho}(t), \hat{H}_0 + \hat{V}_{\text{in}}(t) \right] \\ &\quad + \mathcal{L}_{\text{coll.}}[\hat{\rho}(t)] + \mathcal{L}_{\text{incoh.}}[\hat{\rho}(t)]. \quad (3) \end{aligned}$$

Initially, the field is coupled to the atoms through the interaction Hamiltonian \hat{V} . After tracing out the field degrees of freedom, its role is taken over by two operators $\mathcal{L}_{\text{coll.}}[\hat{\rho}(t)]$ and $\hat{V}_{\text{in}}(t)$. The superoperator $\mathcal{L}_{\text{coll.}}[\hat{\rho}(t)]$ represents collective dissipation caused by the interaction of the atoms with *their own light* from previous passes:

$$\begin{aligned} \mathcal{L}_{\text{coll.}}[\hat{\rho}(t)] &= \frac{\gamma}{2} \sum_{\alpha} \left(\left[\hat{P}_{\alpha}^{(+)} \hat{\rho}(t), \hat{P}_{\alpha}^{(-)} \right] \right. \\ &\quad \left. + \left[\hat{P}_{\alpha}^{(+)} \hat{\rho}(t), \hat{P}_{\alpha}^{(-)} \right] \right), \end{aligned}$$

where $\gamma = 2Q/[V\hbar\varepsilon_0]$, and $\hat{P}_{\alpha}^{(\pm)}$ are components of the vector operators $\hat{\mathbf{P}}^{(\pm)}$. Since the atoms interact with the

¹ In Ref. [53], the atomic sample is positioned at an antinode of a standing wave, which can be taken into account by neglecting $e^{\pm i\mathbf{k}_0\mathbf{r}_a}$.

² $Q/[k_0L]$ is the decay rate of the intensity. The field amplitudes decay two times slower.

light collectively, $\mathcal{L}_{\text{coll.}}[\hat{\rho}(t)]$ eventually involves only the collective dipole moments $\hat{\mathbf{P}}^{(\pm)}$.

If the system is exposed to an *externally applied field* $\mathcal{D}_{\text{in}}(\mathbf{r}, t)$, which is uniform across the atomic ensemble:

$$\mathcal{D}_{\text{in}}(\mathbf{r}, t) = \mathcal{D}_{\text{in}}^{(+)}(t)e^{i\mathbf{k}_0\mathbf{r}} + \mathcal{D}_{\text{in}}^{(-)}(t)e^{-i\mathbf{k}_0\mathbf{r}}, \quad (4)$$

it can be included in the master equation with the interaction Hamiltonian $\hat{V}_{\text{in}}(t)$ constructed similar to $\hat{V}(t)$ in Eq. (2)

$$\hat{V}_{\text{in}}(t) = -\frac{1}{\varepsilon_0} \left(\hat{\mathbf{P}}^{(-)} \mathcal{D}_{\text{in}}^{(+)}(t) + \hat{\mathbf{P}}^{(+)} \mathcal{D}_{\text{in}}^{(-)}(t) \right)$$

The amplitudes $\mathcal{D}_{\text{in}}^{(\pm)}(t)$ can be deterministic complex-valued functions representing classical fields or quantum light in a coherent state. Moreover, $\mathcal{D}_{\text{in}}^{(\pm)}(t)$ can have some statistical distribution that reproduces moments of normal-ordered field operators. The amplitudes $\mathcal{D}_{\text{in}}^{(\pm)}(t)$ allow the inclusion of black-body photons or any arbitrary external field causing stimulated emission.

Besides collective interaction with the radiation, atoms undergo a wide variety of incoherent processes, such as non-radiative decay, ionization. By introducing a separate independent reservoir for each atom and assuming that atoms interact with them identically, we apply the Markovian approximation [57, 58] and derive the most general form of $\mathcal{L}_{\text{incoh.}}[\hat{\rho}(t)]$:

$$\begin{aligned} \mathcal{L}_{\text{incoh.}}[\hat{\rho}(t)] = \frac{1}{2} \sum_{\substack{a,p,q, \\ r,s}} \Gamma_{pqrs}(t) \left([\hat{\sigma}_{a,pq} \hat{\rho}(t), \hat{\sigma}_{a,rs}] \right. \\ \left. + [\hat{\sigma}_{a,pq}, \hat{\rho}(t) \hat{\sigma}_{a,rs}] \right). \quad (5) \end{aligned}$$

The characteristics of the incoherent processes enter the equations through the rates $\Gamma_{pqrs}(t)$.

III. STOCHASTIC EQUATIONS

The master equation (3) is symmetric under atomic permutations. When the system starts from any symmetric density matrix, the problem can be solved for a moderately large number of atoms ($N \lesssim 100$) by applying methods from Refs. [28, 29]. A simplified method from Ref. [27] can be used when the atoms start from a statistical mixture of symmetric pure states and interact only collectively, namely, without $\mathcal{L}_{\text{incoh.}}[\hat{\rho}(t)]$. The main drawback of these methods is their polynomial scaling with N .

The development of our formalism draws inspiration from the concept of a positive P function [36–40] used to generate stochastic differential equations for the problems involving bosonic fields. The final equations possess an intuitive form: the deterministic parts remind classical equations, whereas the quantum effects are attributed to the noise terms.

We attempt to derive similar equations for a compact system of quantum emitters. First, we analyze the distinctions between the quantum description based on the master equation and the semi-classical one based on the Bloch equations [4, 55]. Further, we demonstrate how these equations can be enhanced with supplementary terms, characterized by specific statistical properties, to restore the missing quantum properties.

A. Optical Bloch equations

We start the derivation with the simplest possible ansatz for the density matrix $\hat{\rho}(t)$, assuming a complete factorization of the atomic degrees of freedom in terms of single-particle density matrices $\hat{\rho}_a(t)$:

$$\hat{\rho}(t) = \prod_a \hat{\rho}_a(t). \quad (6)$$

Furthermore, since the system is symmetric under permutations, we assume that all $\hat{\rho}_a(t)$ have the same matrix elements $\rho_{pq}(t)$, so that

$$\hat{\rho}_a(t) = \sum_{pq} \rho_{pq}(t) \hat{\sigma}_{a,pq}.$$

Fig. 1 (a) schematically depicts this ansatz. Although this decomposition is suitable for the assumed initial state of a fully symmetric density matrix of uncorrelated atoms, the further evolution of the system can only be partially captured by this proposed ansatz. To get the equations for the variables $\rho_{pq}(t)$, we generate the following equations for the expectation values $\text{Tr}(\hat{\sigma}_{a,pq} \hat{\rho}(t))$:

$$\frac{d}{dt} \text{Tr}(\hat{\sigma}_{a,pq} \hat{\rho}(t)) = \text{Tr}(\hat{\sigma}_{a,pq} \mathcal{L}[\hat{\rho}(t)]).$$

Assuming the decomposition in Eq. (6), the expectation values $\text{Tr}(\hat{\sigma}_{a,pq} \hat{\rho}(t))$ are equal to $\rho_{qp}(t)$. The considered ansatz for the density matrix factorizes second-order correlators, namely:

$$\text{Tr}(\hat{\sigma}_{a,pq} \hat{\sigma}_{b,rs} \hat{\rho}(t)) = \rho_{qp}(t) \rho_{sr}(t), \quad (7)$$

which leads to a closed system of equations known as Bloch equations [4, 55]:

$$\begin{aligned}
\dot{\rho}_{pq}(t) = & -i\omega_{pq}\rho_{pq}(t) + \frac{1}{2} \sum_{i,j} \left(2\Gamma_{piqj}(t) \rho_{ij}(t) - \Gamma_{ijip}(t) \rho_{jq}(t) - \rho_{pj}(t) \Gamma_{iqij}(t) \right) \\
& + \frac{\gamma}{2} \sum_{r,s} \left(2\rho_{rs}(t) \mathbf{d}_{p<r} \mathbf{d}_{s>q} - \mathbf{d}_{p>r} \mathbf{d}_{r<s} \rho_{sq}(t) - \rho_{pr}(t) \mathbf{d}_{r>s} \mathbf{d}_{s<q} \right) \\
& + \frac{i}{\hbar\varepsilon_0} \mathcal{D}^{(+)}(t) \sum_r \left(\mathbf{d}_{p>r} \rho_{rq}(t) - \rho_{pr}(t) \mathbf{d}_{r>q} \right) + \frac{i}{\hbar\varepsilon_0} \mathcal{D}^{(-)}(t) \sum_r \left(\mathbf{d}_{p<r} \rho_{rq}(t) - \rho_{pr}(t) \mathbf{d}_{r<q} \right),
\end{aligned} \tag{8}$$

where $p > q$ means that index p corresponds to the subset of excited states $\{|e\rangle\}$ and index q represents the subset of ground states $\{|g\rangle\}$. Each atom interacts with the field amplitudes $\mathcal{D}^{(\pm)}(t)$ that combine the incoming fields $\mathcal{D}_{\text{in}}^{(\pm)}(t)$ and the field produced by the other $N - 1$ atoms:

$$\mathcal{D}^{(+)}(t) = \mathcal{D}_{\text{in}}^{(+)}(t) + i\hbar\varepsilon_0 \frac{\gamma}{2} (N - 1) \sum_{e,g} \mathbf{d}_{ge} \rho_{eg}(t), \quad \mathcal{D}^{(-)}(t) = \mathcal{D}_{\text{in}}^{(-)}(t) - i\hbar\varepsilon_0 \frac{\gamma}{2} (N - 1) \sum_{g,e} \mathbf{d}_{eg} \rho_{ge}(t). \tag{9}$$

The factorization of the second-order correlators in Eq. (7) used in the derivations of the Bloch equations shows that these equations are valid only for systems with strong classical behavior. Let us reconstruct the neglected terms in the master equation (3) and analyze their structure. If we insert the decomposition from Eq. (6) in the master equation (3), and then apply Bloch equations (8), we notice that the right-hand side of $\mathcal{L}[\hat{\rho}(t)]$ in Eq. (3) is restored only partially

$$\mathcal{L}[\hat{\rho}(t)] - \frac{d\hat{\rho}(t)}{dt} = \sum_{b \neq c} \hat{\chi}_{b,c}(t) \prod_{a \neq b,c} \hat{\rho}_a(t). \tag{10}$$

This is schematically depicted in Figs. 1 (b) and (c). The time derivative of Eq. (6) can generate the terms, where only one $\hat{\rho}_a$ is modified. Consequently, the remaining terms in Eq. (10) entangle pairs of $\hat{\rho}_a$ through $\hat{\chi}_{b,c}(t)$ defined as follows:

$$\hat{\chi}_{b,c}(t) = \sum_{p,q,r,s} \chi_{pqrs}(t) \hat{\sigma}_{b,pq} \hat{\sigma}_{c,rs}, \tag{11}$$

where

$$\begin{aligned}
\chi_{pqrs}(t) = & \frac{\gamma}{2} \left[\left(\sum_{r'} \rho_{pr'}(t) \mathbf{d}_{r'>q} - \rho_{pq}(t) \sum_{g,e} \mathbf{d}_{eg} \rho_{ge}(t) \right) \sum_{p'} \left(\mathbf{d}_{r<p'} \rho_{p's}(t) - \rho_{rp'}(t) \mathbf{d}_{p'<s} \right) \right. \\
& \left. + \sum_{r'} \left(\rho_{pr'}(t) \mathbf{d}_{r'>q} - \mathbf{d}_{p>r'} \rho_{r'q}(t) \right) \left(\sum_{p'} \mathbf{d}_{r<p'} \rho_{p's}(t) - \rho_{rs}(t) \sum_{e,g} \mathbf{d}_{ge} \rho_{eg}(t) \right) \right] + [p, q \rightleftharpoons r, s].
\end{aligned} \tag{12}$$

B. Stochastic terms

Although $\chi_{pqrs}(t)$ looks complicated, the uncompensated terms in the right-hand side of Eq. (10) contain only entangled pairs of atoms, as Eq. (11) suggests. Non-trivial correlations of higher orders are not involved, so the terms in Eq. (11) can be correctly recaptured by adding appropriate stochastic terms to the Bloch equations (8). In addition to the deterministic time evolution, we introduce stochastic terms F_{pq} as described by the following equation:

$$\dot{\rho}_{pq}(t) \Big|_{\text{noise}} = F_{pq}(\{\rho_{ij}(t)\}, t). \tag{13}$$

It is important to note that the properties of the noise terms can be generally parametrized by the dynamic vari-

ables $\rho_{ij}(t)$. We only constrain F_{pq} to be Gaussian white noise terms with zero mean and the following second-order correlation properties:

$$\begin{aligned}
\langle F_{pq}(\{x_{ij}\}, t) F_{rs}(\{x_{ij}\}, t') \rangle \\
= \kappa_{pqrs}(\{x_{ij}\}, t) \delta(t - t'). \tag{14}
\end{aligned}$$

The coefficients κ_{pqrs} will be specified later. Note that Eq. (14) is parameterized by x_{ij} , which does not represent dynamic variables $\rho_{ij}(t)$, unlike, for instance, in Eq. (13). When included in the noise terms, the dynamic variables $\rho_{ij}(t)$ contribute their own statistics. To capture the statistical properties inherent solely in the noise terms F_{pq} , Eq.(14) is formulated without explicit dependence on $\rho_{ij}(t)$.

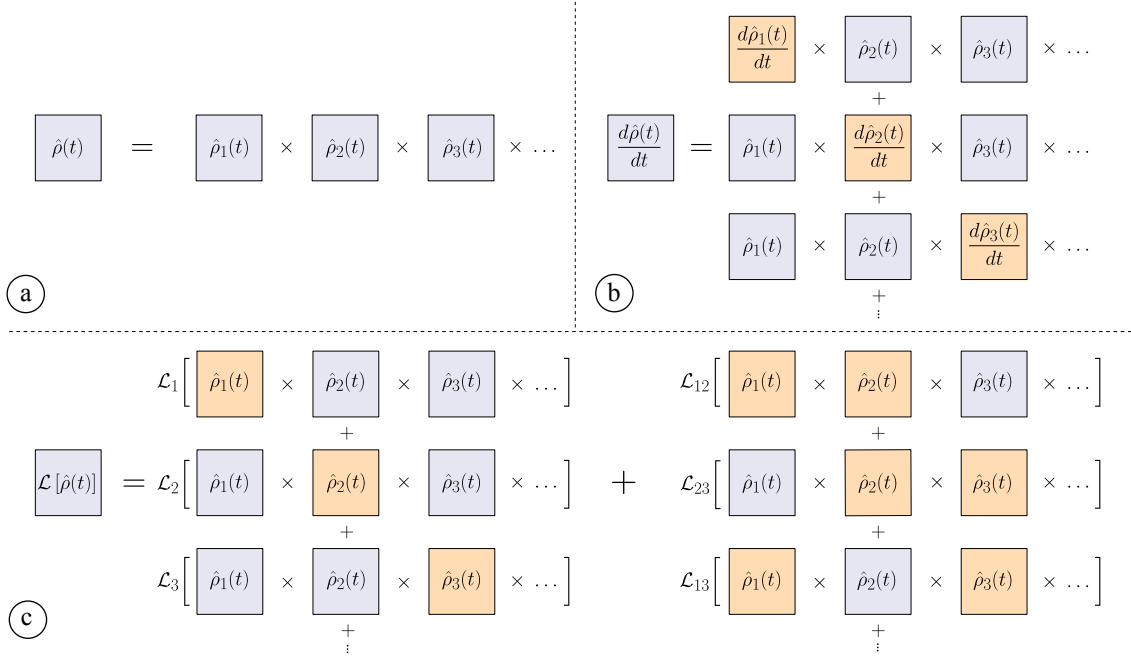


FIG. 1. Schematic representation of the completely factorized density matrix (a) and its interaction with the time derivative (b) and $\mathcal{L}[\hat{\rho}(t)]$ (c). In panel (a), we illustrate the density matrix of the whole ensemble as a product state composed of individual single-particle density matrices. The time derivative of this density matrix leads to a sum of products, where only single-particle density matrices are affected, as highlighted by the orange color in panel (b). Upon applying the collective Liouville operator, in addition to products where only a single particle is affected $\mathcal{L}_a[\dots]$, there is an additional contribution from two-particle interactions $\mathcal{L}_{a \neq b}[\dots]$. This is represented in panel (c).

We assume that the noise terms are integrated in Itô's sense. Typically, the stochastic equations are solved with the Monte Carlo approach. The proper statistics of the dynamic variables $\rho_{pq}(t)$ is reconstructed by repeatedly solving equations with a randomly sampled stochastic contribution in accordance with their statistical properties. Since the variables are independently integrated for each repetition, the problem is parallelizable, which gives a great advantage in performance compared to the methods based on the direct decomposition of the quantum state in some basis set.

To reconstruct the density matrix $\hat{\rho}(t)$, we insert each realization of the variables $\rho_{pq}(t)$ into the decomposition in Eq. (6) and aggregate all realizations of density matrices (6) into a normalized linear combination:

$$\begin{aligned} \hat{\rho}(t) &= \left\langle \prod_a \hat{\rho}_a(t) \right\rangle = \left\langle \prod_a \sum_{pq} \rho_{qp}(t) \hat{\sigma}_{a,pq} \right\rangle \\ &= \sum_i \left[\prod_a \sum_{pq} \rho_{qp}^{(i)}(t) \hat{\sigma}_{a,pq} \right] / N_{\text{sample}}. \end{aligned} \quad (15)$$

This density matrix is no longer factorizable. Here, $\rho_{qp}^{(i)}(t)$ represents the i -th realization of the variables $\rho_{qp}(t)$, and N_{sample} is the total number of statistical realizations. We anticipate that this linear combination can restore missing entangled terms in Eq. (10). The remaining step is to identify a specific expression for $\kappa_{pqrs}(t)$.

Although the new decomposition in Eq. (15) does not change the expression for the first term $\mathcal{L}[\hat{\rho}(t)]$, the derivative $\frac{d\hat{\rho}(t)}{dt}$ is modified by additional terms proportional to κ_{pqrs} , due to Itô's lemma. Consider an arbitrary function S that depends on variables $\rho_{pq}(t)$. If the variables $\rho_{pq}(t)$ are governed by equations that include the noise terms from Eq. (13), Itô's lemma can be expressed as:

$$\frac{dS}{dt} = \sum_{p,q} \frac{\partial S}{\partial \rho_{pq}} \frac{d\rho_{pq}}{dt} + \frac{1}{2} \sum_{p,q,r,s} \frac{\partial^2 S}{\partial \rho_{pq} \partial \rho_{rs}} \kappa_{pqrs}. \quad (16)$$

Consequently, the full derivative of the density matrix in Eq. (15) acquires the following additional contribution:

$$\begin{aligned} \frac{d\hat{\rho}(t)}{dt} &= \dots \\ &+ \left\langle \sum_{b \neq c} \sum_{p,q,r,s} \kappa_{pqrs}(\{\rho_{ij}(t)\}, t) \hat{\sigma}_{b,pq} \hat{\sigma}_{c,rs} \prod_{a \neq b,c} \hat{\rho}_a(t) \right\rangle, \end{aligned}$$

that entangles pairs of atoms and has exactly the same form as the right-hand side of Eq. (10). Consequently, if the correlators of the noise terms are

$$\kappa_{pqrs} = \chi_{pqrs},$$

the Bloch equations (8) supplemented by the noise terms from Eq. (13) fully satisfy the master equation (3).

To simulate F_{pq} numerically, we have to decompose them in terms of independent noise terms. There is no

unique decomposition, however, the structure of Eq. (12) suggests the most compact one, given by the following expression:

$$\begin{aligned}
F_{pq}(\{\rho_{ij}(t)\}, t) = & \sqrt{\frac{\gamma}{2}} \sum_r \left[\left(\mathbf{d}_{p<r} \rho_{rq}(t) - \rho_{pr}(t) \mathbf{d}_{r<q} \right) \mathbf{f}(t) + \left(\rho_{pr}(t) \mathbf{d}_{r>q} - \mathbf{d}_{p>r} \rho_{rq}(t) \right) \mathbf{g}(t) \right] \\
& + \sqrt{\frac{\gamma}{2}} \left(\sum_r \rho_{pr}(t) \mathbf{d}_{r>q} - \rho_{pq}(t) \sum_{g,e} \mathbf{d}_{eg} \rho_{ge}(t) \right) \mathbf{f}^\dagger(t) + \sqrt{\frac{\gamma}{2}} \left(\sum_r \mathbf{d}_{p<r} \rho_{rq}(t) - \rho_{pq}(t) \sum_{e,g} \mathbf{d}_{ge} \rho_{eg}(t) \right) \mathbf{g}^\dagger(t),
\end{aligned} \tag{17}$$

where we introduce vectors $\mathbf{f}(t)$, $\mathbf{f}^\dagger(t)$, $\mathbf{g}(t)$, $\mathbf{g}^\dagger(t)$ whose components are Gaussian white noise terms independent of the dynamic variables $\rho_{rq}(t)$. The vectors $\mathbf{f}(t)$, $\mathbf{f}^\dagger(t)$ are statistically independent from the vectors $\mathbf{g}(t)$, $\mathbf{g}^\dagger(t)$. The vectors $\mathbf{f}(t)$, $\mathbf{f}^\dagger(t)$ have the correlation properties

$$\begin{aligned}
\langle f_\alpha(t) f_\beta(t') \rangle &= \langle f_\alpha^\dagger(t) f_\beta^\dagger(t') \rangle = 0, \\
\langle f_\alpha(t) f_\beta^\dagger(t') \rangle &= \delta_{\alpha\beta} \delta(t - t'),
\end{aligned} \tag{18}$$

that can only be sampled by complex-valued Gaussian white noise terms. Corresponding stochastic properties hold for $\mathbf{g}(t)$ and $\mathbf{g}^\dagger(t)$. The number of the components of the vectors $\mathbf{f}(t)$, $\mathbf{f}^\dagger(t)$, $\mathbf{g}(t)$, $\mathbf{g}^\dagger(t)$ is defined by the dimensionality of the dipole moment vector \mathbf{d}_{eg} . Eq. (18) does not uniquely define the form of the noise terms. One can simply choose $\mathbf{f}^\dagger(t)$, $\mathbf{g}^\dagger(t)$ to be complex conjugates of $\mathbf{f}(t)$, $\mathbf{g}(t)$. Another freedom is given by rescaling of the noise terms: if $\mathbf{f}(t)$ is divided and $\mathbf{f}^\dagger(t)$ is multiplied by the same number, the statistical properties in Eq. (18) are preserved. This freedom of choice is equivalent to the diffusion gauge in the context of positive P representation formalism [43]. The way we fix the form of the elementary noise terms $\mathbf{f}(t)$, $\mathbf{f}^\dagger(t)$, $\mathbf{g}(t)$, $\mathbf{g}^\dagger(t)$ is discussed in Sec. III C.

Adding the noise terms enriches the Bloch equations with the spontaneous nature of the quantum mechanics, allowing a correct treatment of the spontaneous emission — an indispensable triggering process of superfluorescence. As mentioned in the introduction, many authors recognized the importance of adding stochastic terms into semi-classical equations by different phenomenological approaches [30–33]. Our approach is based on rigorous derivation and hence can serve as a base for further investigations and approximate methods.

Note that the noise decomposition in Eq. (17) conserves the “trace” of the effective density matrix $\rho_{pq}(t)$

$$\sum_p \dot{\rho}_{pp}(t) = \sum_p F_{pp}(\{\rho_{ij}(t)\}, t) = 0.$$

This property is important for generating compact expressions for the expectation values. Based on the decomposition in Eq. (15), one can show that the one and

two-particle expectation values possess intuitive expressions in terms of the statistical variables $\rho_{pq}(t)$:

$$\begin{aligned}
\text{Tr}(\hat{\sigma}_{a,pq} \hat{\rho}(t)) &= \langle \rho_{qp}(t) \rangle, \\
\text{Tr}(\hat{\sigma}_{a,pq} \hat{\sigma}_{b,rs} \hat{\rho}(t)) &= \langle \rho_{qp}(t) \rho_{sr}(t) \rangle,
\end{aligned} \tag{19}$$

where $a \neq b$. Similar expressions hold for high-order correlation functions.

C. Stochastic freedom

Unfortunately, the stochastic terms $F_{pq}(t)$ break an important property of the variables $\rho_{pq}(t)$ expected from the original, deterministic Bloch equations. Starting from Hermitian initial conditions, the Bloch equations preserve the Hermiticity of the variables $\rho_{pq}(t)$. By Hermiticity, we henceforth refer to the condition where $\rho_{pq}(t) = \rho_{qp}^*(t)$. However, in order to sample the correlator $\chi_{pqrs}(t)$, the noise terms must be non-Hermitian, that is, $F_{pq}(t) \neq F_{qp}^*(t)$, which makes the dynamic variables $\rho_{pq}(t)$ non-Hermitian as well, namely $\rho_{pq}(t)^* \neq \rho_{qp}(t)$. Breaking of the Hermiticity comes with the drawback of diverging behavior of the solutions of the Bloch equations. Even without any noise terms, the original Bloch equations written for non-Hermitian variables may lead to unstable solutions with hyperbolic divergence:

$$\rho_{pq}(t) \sim \frac{1}{t - t_0}.$$

As the singularity is approached, the dynamic variables become anti-Hermitian, that is, $\rho_{eg}(t) = -\rho_{ge}^*(t)$. Consequently, attempting to simulate Eq. (8) with the noise terms in Eq. (17) leads to an unstable temporal dependence of expectation values, as demonstrated in Fig. 2.

In the context of the positive P representation, the same stability issues are encountered, which motivated the development of so-called stochastic gauges [42, 43]. In Appendix A, we adopt these stochastic gauges for our formalism. In particular, we reproduce the most useful drift gauges in Appendix B. By applying drift gauges, we can modify deterministic parts of the stochastic equations. In exchange, we have to introduce a weight coefficient $\Omega(t) = e^{C_0(t)}$ in the decomposition of the density

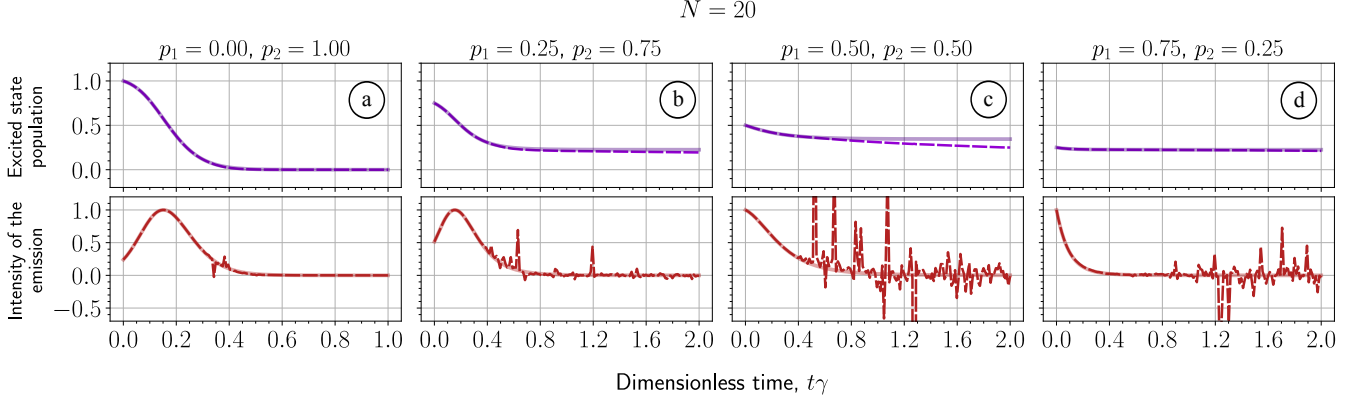


FIG. 2. Solution of the non-modified set of equations (8) with the noise terms in Eq. (17) (opaque lines) compared with the exact solution based on Ref. [28] (semi-transparent lines) for $N = 20$ identical two-level atoms. We vary the parameters p_1 and p_2 which define the initial probabilities of finding an atom in the ground and excited states, respectively. The initial non-diagonal density matrix elements are zero $\rho_{12}(0) = \rho_{21}(0) = 0.0$ and the populations are $\rho_{11}(0) = p_1$ and $\rho_{22}(0) = p_2$. The intensity of the emission is normalized to the maximum value. For each plot, we average over 10^5 stochastic realizations.

matrix in Eq. (15):

$$\hat{\rho}(t) = \left\langle \Omega(t) \prod_a \sum_{pq} \rho_{qp}(t) \hat{\sigma}_{a,pq} \right\rangle. \quad (20)$$

This change is also reflected in the expressions for the expectation values in Eq. (19):

$$\begin{aligned} \text{Tr}(\hat{\sigma}_{a,pq} \hat{\rho}(t)) &= \langle \Omega(t) \rho_{qp}(t) \rangle, \\ \text{Tr}(\hat{\sigma}_{a,pq} \hat{\sigma}_{b,rs} \hat{\rho}(t)) &= \langle \Omega(t) \rho_{qp}(t) \rho_{sr}(t) \rangle, \end{aligned} \quad (21)$$

where $a \neq b$. The form of the equation for the weight coefficient directly depends on how we modify the deterministic parts.

The modification of the deterministic part of the Bloch equations should prevent the unbounded growth of the dynamic variables $\rho_{pq}(t)$. When the Bloch equations are applied to Hermitian initial conditions without additional noise terms, they do not exhibit divergent behavior. However, as mentioned earlier, when the dynamic variables are not perfectly Hermitian, divergent solutions can be encountered. Fortunately, these equations can be slightly modified to ensure that non-Hermiticity does not lead to any instability. The diverging solutions can be completely eliminated by implementing the following substitution in Eq. (9):

$$\begin{aligned} \sum_{g,e} \mathbf{d}_{eg} \rho_{ge}(t) &\rightarrow \frac{1}{2} \sum_{g,e} \mathbf{d}_{eg} (\rho_{ge}(t) + \rho_{eg}^*(t)), \\ \sum_{e,g} \mathbf{d}_{ge} \rho_{eg}(t) &\rightarrow \frac{1}{2} \sum_{e,g} \mathbf{d}_{ge} (\rho_{eg}(t) + \rho_{ge}^*(t)). \end{aligned} \quad (22)$$

The fields become Hermitian after this substitution, namely $\mathcal{D}^{(+)}(t) = \mathcal{D}^{(-)*}(t)$. In return, we introduce the weight coefficient $\Omega(t) = e^{C_0(t)}$. The coefficient $C_0(t)$

starts from zero and satisfies the following equation:

$$\begin{aligned} \frac{dC_0(t)}{dt} &= \frac{N-1}{2} \sqrt{\frac{\gamma}{2}} \sum_{g,e} \left[\mathbf{f}^\dagger(t) \mathbf{d}_{eg} (\rho_{ge}(t) - \rho_{eg}^*(t)) \right. \\ &\quad \left. + \mathbf{g}^\dagger(t) \mathbf{d}_{ge} (\rho_{eg}(t) - \rho_{ge}^*(t)) \right]. \end{aligned} \quad (23)$$

Note that the right-hand side of this equation is proportional to the anti-Hermitian parts of the variables $\rho_{pq}(t)$. Since the weight coefficient $\Omega(t)$ involves the exponentiation of $C_0(t)$, which is itself proportional to $(N-1)$, $\Omega(t)$ can rapidly grow over time. Consequently, the averaging in Eq. (21) may require a large number of statistical realizations to converge. To reduce the need for the proposed drift gauge, we introduce two additional techniques.

First, we notice that the drift gauge is not always required since the original equations do not always increase the anti-Hermitian parts of the dynamic variables. We can apply the drift gauge once the relative increase of the anti-Hermitian parts per time step exceeds a certain limit. In practice, we have found that gauging is only needed when the effective population inversions are not negative, i.e., $\text{Re}[\rho_{ee}(t) - \rho_{gg}(t)] \geq 0$ for any excited state $|e\rangle$ and ground state $|g\rangle$. Since the variables are complex at the level of single trajectories, we take the real parts of the populations.

In the context of superfluorescence, the positive sign of the population inversions causes exponential amplification of the field components $\mathcal{D}_\alpha^{(\pm)}(t)$, whereas negative population inversions lead to their absorption. Consequently, positive population inversions increase both the Hermitian and anti-Hermitian parts of the field components, which can trigger diverging behavior. Negative population inversions, in contrast, reduce the fields and their anti-Hermitian parts, making gauging unnecessary.

A second technique is based on the flexibility provided by the correlation properties of the elementary noise vectors $\mathbf{f}(t)$, $\mathbf{f}^\dagger(t)$, $\mathbf{g}(t)$, and $\mathbf{g}^\dagger(t)$. In Eq. (18), we have

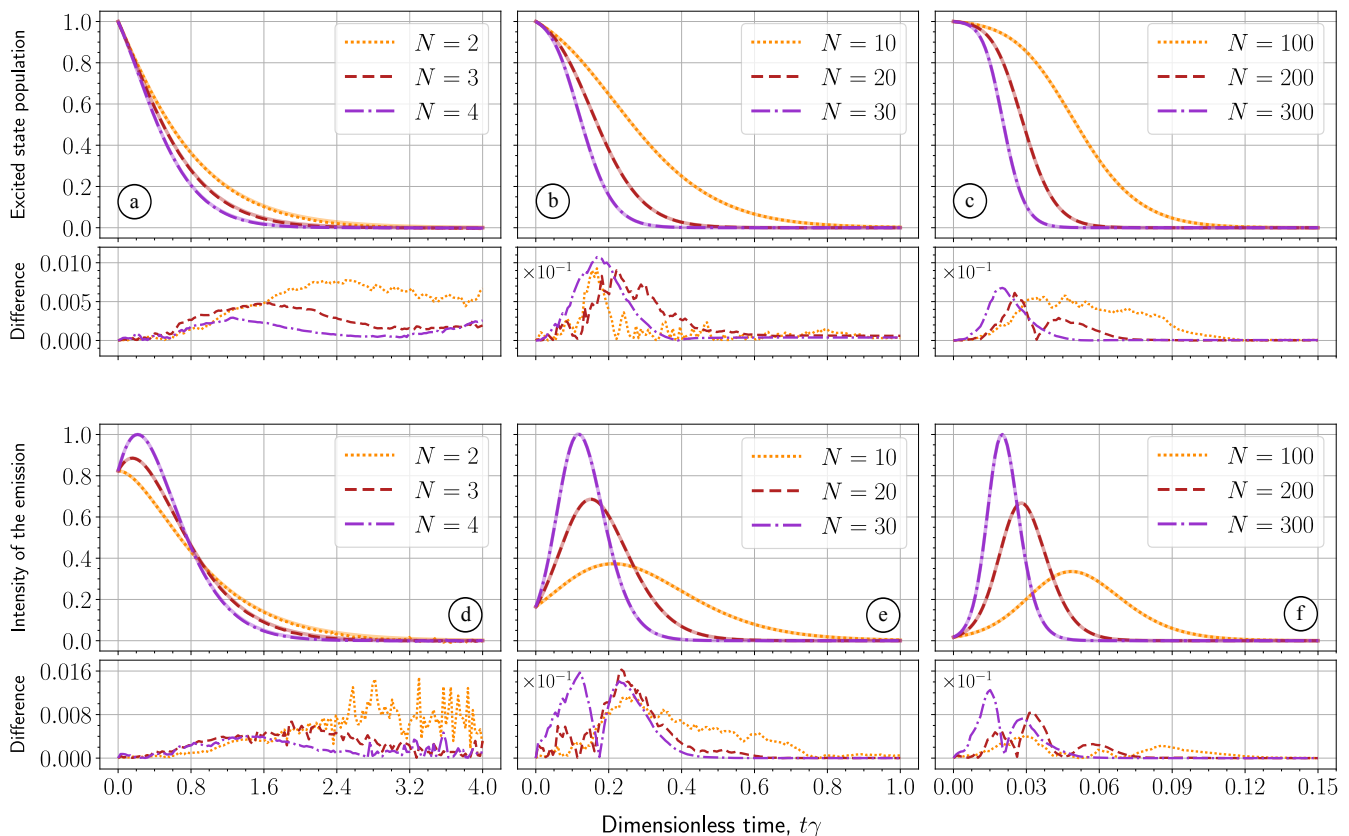


FIG. 3. Solutions to the stochastic equations, modified as described in Sec. III C. The semi-transparent lines correspond to quantum expectation values, while the opaque lines represent stochastic averages. The intensities (d, e, f) have been normalized to the maximum. The subplots below each row show the absolute difference between stochastic averages and quantum expectation values. We label some plots with $\times 10^{-1}$ to highlight that the corresponding values should be multiplied by this factor. Each plot involves averaging over 10^5 stochastic realizations. For the cases of $N = 2, 3, 4$ (a, d), we have omitted 18, 4, 2 unstable trajectories, respectively.

only outlined their correlation properties without prescribing any specific form. As mentioned before, there is no unique way to define them. One of the possible representations, which we later employ in the numerical simulations, takes the following form:

$$\begin{aligned} f_\alpha(t) &= \eta_\alpha(t) \bar{f}_\alpha(t), & f_\alpha^\dagger(t) &= \eta_\alpha^{-1}(t) \bar{f}_\alpha^*(t), \\ g_\alpha(t) &= \theta_\alpha(t) \bar{g}_\alpha(t), & g_\alpha^\dagger(t) &= \theta_\alpha^{-1}(t) \bar{g}_\alpha^*(t), \end{aligned} \quad (24)$$

where $\theta_\alpha(t)$ and $\eta_\alpha(t)$ can take on any values. The only constraint is that they must be statistically independent of the noise terms from the future. Eq. (24) explicitly associates the noise terms $\mathbf{f}(t)$ and $\mathbf{f}^\dagger(t)$ with a single vector of independent complex noise terms $\bar{\mathbf{f}}(t)$. Similarly, $\mathbf{g}(t)$ and $\mathbf{g}^\dagger(t)$ are linked to $\bar{\mathbf{g}}(t)$. These new noise terms, $\bar{\mathbf{f}}(t)$ and $\bar{\mathbf{g}}(t)$, consist of independent and normal Gaussian white real noise terms $\bar{\mathbf{f}}_1(t)$, $\bar{\mathbf{f}}_2(t)$, $\bar{\mathbf{g}}_1(t)$, and $\bar{\mathbf{g}}_2(t)$:

$$\begin{aligned} \bar{\mathbf{f}}(t) &= \frac{1}{\sqrt{2}} (\bar{\mathbf{f}}_1(t) + i\bar{\mathbf{f}}_2(t)), \\ \bar{\mathbf{g}}(t) &= \frac{1}{\sqrt{2}} (\bar{\mathbf{g}}_1(t) + i\bar{\mathbf{g}}_2(t)). \end{aligned} \quad (25)$$

The explicit representation in Eq. (24) preserves the correlation properties in Eq. (18) regardless of the form of $\theta_\alpha(t)$ and $\eta_\alpha(t)$. To reduce the need for the drift gauge presented in Eq. (22), we fix the form of the functions $\theta_\alpha(t)$ and $\eta_\alpha(t)$ in such a way that the anti-Hermitian parts of the dipole moments

$$\left| \sum_{g,e} d_{eg,\alpha} (\rho_{ge}(t) - \rho_{eg}^*(t)) \right| \quad (26)$$

are minimized for each component α . The resulting expressions for $\theta_\alpha(t)$ and $\eta_\alpha(t)$ can be found in Appendix C.

IV. NUMERICAL ANALYSIS

We illustrate the proposed formalism through a series of numerical examples. The deterministic components of the stochastic equations are numerically integrated using the adaptive step-size method `Tsit5`, which is implemented in the `DifferentialEquations.jl` library [59].

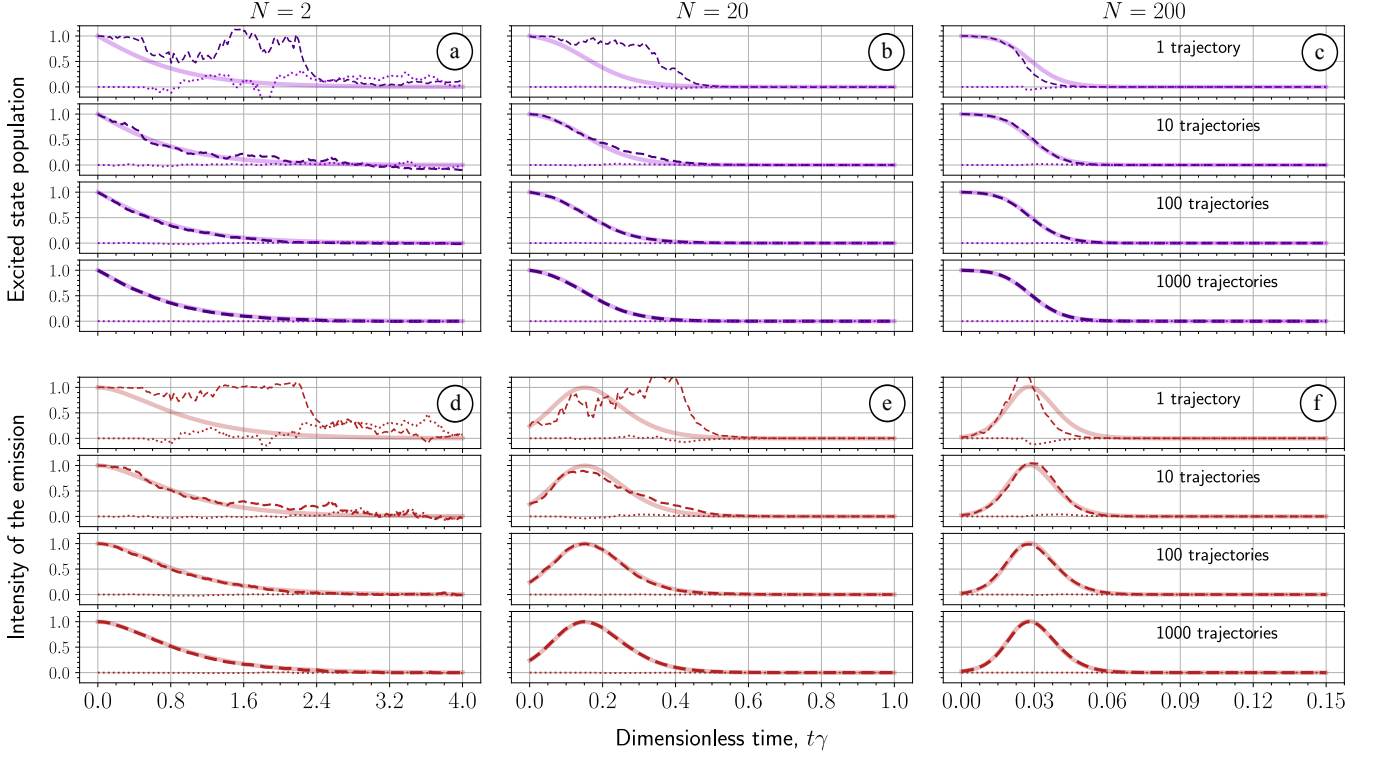


FIG. 4. Convergence of the stochastic averages (dashed lines) to the exact quantum expectation values (solid lines) for different numbers of atoms N . The atomic ensemble is initially fully excited, i.e. $\rho_{22}(0) = 1.0$, and other matrix elements are zero. The observables chosen here are the probability of finding an excited atom (a, b, c) and the intensity of the emitted field (d, e, f). Intensity is normalized to the maximum. The dotted lines represent the imaginary parts of corresponding quantities. As expected, they disappear with the increasing number of trajectories.

The noise components are integrated using the Euler-Maruyama method. For both methods, the maximum allowed timestep was limited to approximately $T_{\max}/10^4$ for two-level systems and $T_{\max}/10^3$ for three-level systems. Here, T_{\max} represents the last point on the dimensionless time grid.

Before we proceed with numerical simulations, let us link the expectation values of quantum-mechanical operators with the respective stochastic variables. Specifically, we will examine the average populations of atomic levels using the following expression:

$$p_q(t) = \frac{1}{N} \sum_a \text{Tr}(\hat{\sigma}_{a,pp} \hat{\rho}(t)) = \langle \Omega(t) \rho_{pp}(t) \rangle,$$

where Eq. (20) has been utilized.

In compact systems, the field properties can be expressed through the atomic operators and, consequently, through the associated stochastic variables. Up to an insignificant factor, the intensity of the emission polarized along the α -axis is given by the product of collective dipole moments:

$$I_\alpha(t) = \text{Tr} \left[\hat{P}_\alpha^{(-)} \hat{P}_\alpha^{(+)} \hat{\rho}(t) \right] \quad (27a)$$

Utilizing Eq. (20), we express the intensities $I_\alpha(t)$ in

terms of the stochastic variables $\rho_{pq}(t)$:

$$I_\alpha(t) = N \sum_{e_1, e_2, g} d_{e_1 g, \alpha} d_{g e_2, \alpha} \langle \Omega(t) \rho_{e_2 e_1}(t) \rangle + N(N-1) \sum_{\substack{e_1, e_2 \\ g_1, g_2}} d_{e_1 g_1, \alpha} d_{g_1 e_1, \alpha} \langle \Omega(t) \rho_{g_2 e_2}(t) \rho_{e_2 g_2}(t) \rangle. \quad (27b)$$

The full intensity is found by summing all the components.

A. Cooperative emission of two-level atoms

Let us revisit the example of identical two-level atoms collectively interacting with their own field. The ground state manifold $|g\rangle$ collapses to a single state $|1\rangle$, and correspondingly, the excited state manifold $|e\rangle$ reduces to a single state $|2\rangle$. The initial set of stochastic equations exhibits unstable behavior as illustrated in Fig. 2. To resolve this, we modify the equations according to Eq. (22), namely by making the deterministic part of the field Hermitian. This adjustment requires the introduction of an additional variable $C_0(t)$ which re-weights the trajectories, as shown in Eq. (20). Additionally, we employ the

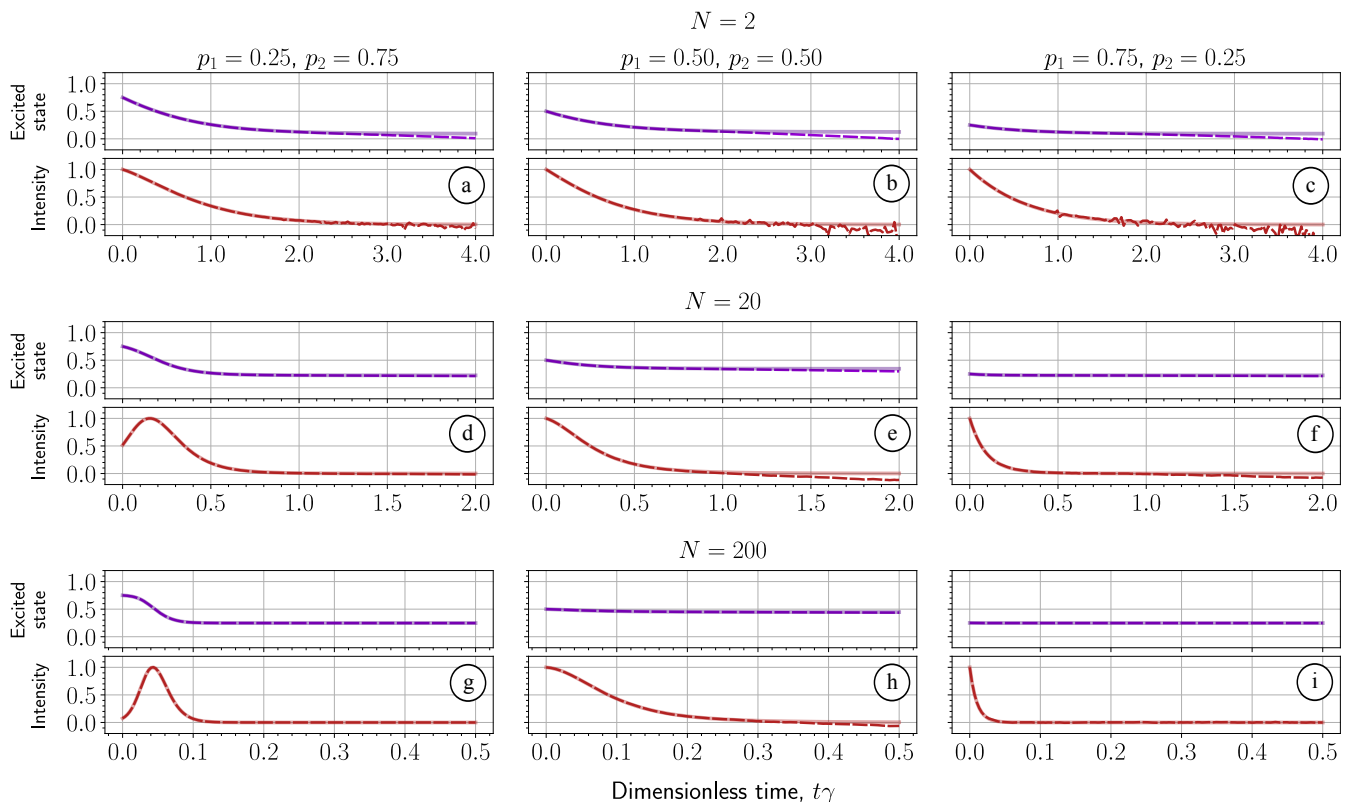


FIG. 5. The excited state population and emission intensity plotted for different numbers of atoms N and varying initial conditions. The semi-transparent lines correspond to the quantum expectation values, while the opaque lines represent the stochastic averages. We averaged over 10^5 stochastic trajectories. However, for the case of $N = 2$, we excluded 208, 304, and 270 unstable trajectories corresponding to initial conditions with p_2 values of 0.75 (a), 0.50 (b), and 0.25 (c) respectively. For all other parameter sets, no diverging trajectories were encountered.

diffusion gauge presented in Eq. (24) and Appendix C to suppress the increase of non-Hermitian dipole moment components.

When the ensemble starts from the fully excited state, characterized by $\rho_{22}(0) = 1.0$, with all other matrix elements set to zero, the phenomenon of superradiance is observed. Fig. 3 shows the excited state population and emission intensity for different numbers of atoms N . We exclude the single-atom case $N = 1$ since it does not require the extension of the ansatz (6) beyond the single-particle density matrix. Thus, the noise terms are unnecessary in this case. Increasing the value of N leads to faster depopulation of the excited state and a narrower, more pronounced peak in intensity. For the number of atoms $N \gtrsim 10$, the discrepancy between stochastic averages and quantum expectation values remains within the range of 0.1%-0.2%, i.e., at the level of statistical fluctuations. However, for smaller N , this difference is increased by an order of magnitude. From our experience, this discrepancy appears systematically in cases where the non-linear noise terms become as significant as the deterministic part.

In Fig. 3 we used 10^5 stochastic realizations. In practice, much fewer trajectories are required for the con-

vergence of selected observables. Fig. 4 demonstrates the convergence of population and intensity for different numbers of stochastic realizations. For qualitative analysis, averaging over 10^2 trajectories is enough, while averaging over 10^3 trajectories already gives accurate averages. In addition to the direct comparison with quantum averages, we use another criterion of convergence: imaginary parts of such observables as populations or intensities should vanish after averaging. For a single trajectory, the imaginary part is comparable to the real part, thus it does not have physical meaning. Statistical averages represent observables only after averaging over a significant amount of trajectories.

There is a special case when the initial state is statistically mixed. As shown in Ref. [28], if the system is prepared in the state without coherences $\rho_{12}(0) = \rho_{21}(0) = 0.0$ and only with the diagonal elements:

$$\rho_{11}(0) = p_1, \quad \rho_{22}(0) = p_2, \quad (28)$$

with $p_2 < 1.0$, the collective emission process is suppressed. The ensemble reaches a steady state with a nonzero probability of finding an excited atom, namely

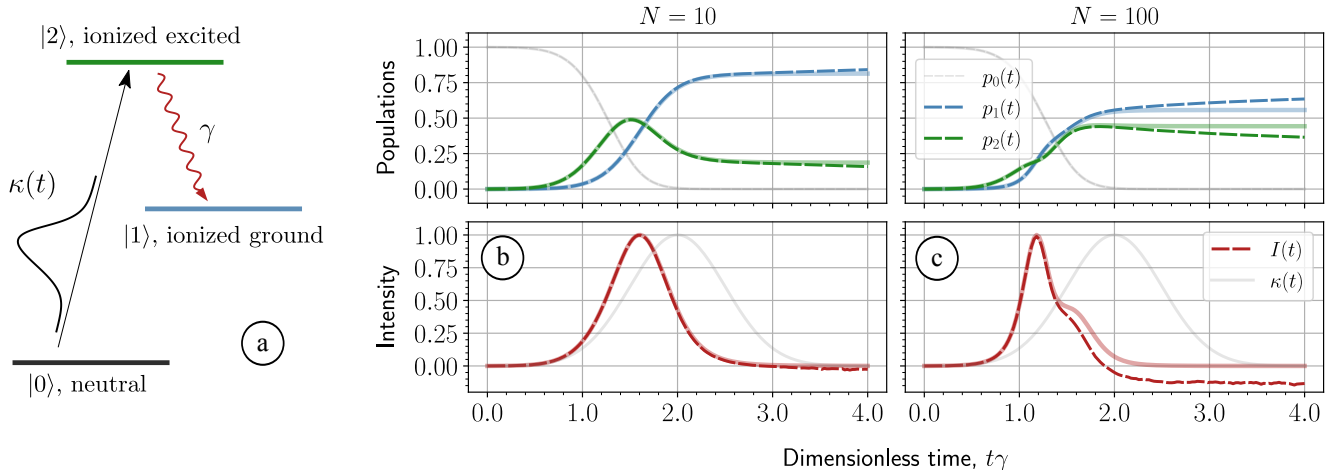


FIG. 6. (a) Level structure of the pumped two-level atoms. Neutral atoms are photoionized by a pump pulse with a profile $\kappa(t)$. Excited ions relax via collective emission $2 \rightarrow 1$ with a rate γ . We compare the stochastic (opaque lines) and quantum (semi-transparent lines) expectation values for two cases: $N = 10$ (b) and $N = 100$ (c). We have selected a Gaussian envelope for the pump, $\kappa(t) = I_p \exp[-(t-t_0)^2/2\tau^2] / \sqrt{2\pi\tau^2}$, with the following parameters used for calculations: $I_p = 10$, $t_0 = 2.0/\gamma$, and $\tau = 0.5/\gamma$.

$\langle \rho_{22}^{(ss)} \rangle > 0$, where ss stands for steady state³. In this steady state, the field intensity, as defined in Eq. (27), is zero, implying that:

$$\langle \rho_{22}^{(ss)} \rangle + (N - 1) \langle \rho_{12}^{(ss)} \rho_{21}^{(ss)} \rangle = 0. \quad (29)$$

This, in turn, implies that $\langle \rho_{12}^{(ss)} \rho_{21}^{(ss)} \rangle < 0$, a condition that can only be met when the dipole moments exhibit significant non-Hermitian behavior at the level of individual stochastic realizations. Our gauges aim to minimize the non-Hermitian components, and finding appropriate gauging to account for this particular case remains a separate challenge. And indeed, this special case is not fully reproduced by the stochastic equations, see Fig. 5. For a small number of atoms $N = 2$, the excited state population does not converge to the correct curve, while the intensity exhibits slow convergence and noisy behavior at later time moments. The situation improves as the number of atoms increases. For $N = 20$, the case with $p_2 = 0.75$ is well reproduced, without the spikes in the intensity as in Fig. 2 (b). Furthermore, for a large number of atoms $N = 200$, the curves corresponding to no population inversion $p_2 = 0.25$ also converge to correct ones. However, the case with $p_2 = 0.5$ still has some issues with intensity since it goes below zero. In Ref. [28], an analytical expression for the steady-state density matrix was found. Initial conditions enter this expression as a single parameter $(p_1 p_2) \leq 1/4$, and the larger this parameter, the stronger the population trapping effect becomes. This explains the issues with $p_1 = p_2 = 0.5$ for any number of atoms in Fig. 5 (b, e, h).

The population trapping effect occurs due to the assumption that all the atoms experience the same field. This field is immediately updated according to the current value of the dipole moments. At some point, the emission and absorption processes balance each other, and the ensemble does not relax to the ground state but rather evolves into a quasi-stationary state.

B. Incoherent pumping

In a more realistic situation, the excitation of the ensemble is not instantaneous. The system's initial condition may be prepared by continuous incoherent pumping, as in X-ray lasing experiments [22, 60]. A pump pulse ionizes neutral atoms, opening the lasing transition in the ionized atoms, see Fig. 6 (a) for a sketch of the level structure. In Ref. [28], it was shown that if the system is pumped incoherently, it reaches a steady state similar to the ones in Fig. 5, in which the atoms are not fully relaxed.

At the level of stochastic equations, the additional variable describing the population of the neutral state is required, denoted by $\rho_{00}(t)$. This state is coupled to the excited state only through the incoherent pumping $0 \rightarrow 2$ with the rate $\Gamma_{2020}(t) = \kappa(t)$. The time dependence of $\kappa(t)$ defines the pump profile. Pumping results in an additional term in equation for $\rho_{22}(t)$:

$$\dot{\rho}_{22}(t) = \dots + \kappa(t) \rho_{00}(t),$$

³ Here, in averages we dropped out the weight function for brevity.

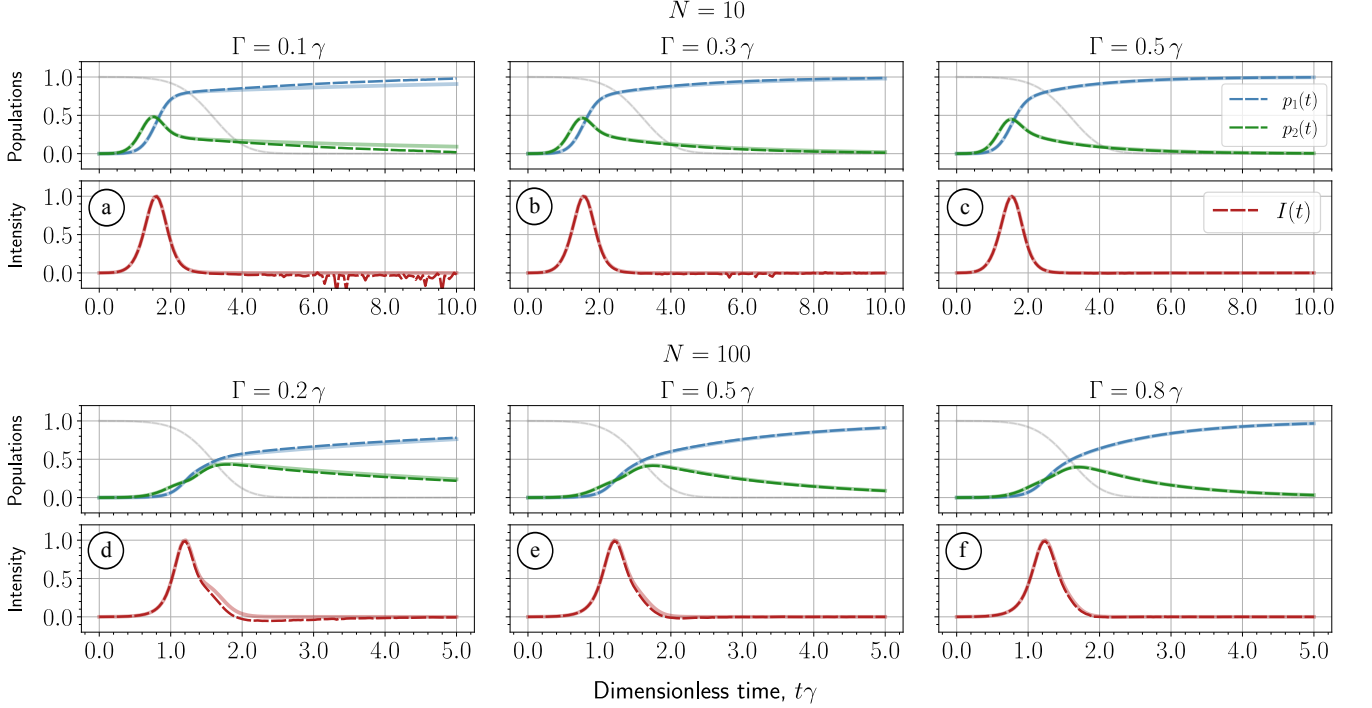


FIG. 7. Regularization of the incoherently pumped system from Fig. 6 by introducing an additional non-radiative dissipation channel $2 \rightarrow 1$ with a rate Γ . The semi-transparent lines correspond to quantum expectation values, while the opaque lines represent stochastic averages. We averaged over 10^5 trajectories. For the case of $N = 10$, we omitted 53, 7, and 2 trajectories for $\Gamma = 0.1\gamma$ (a), 0.3γ (b), and 0.5γ (c), respectively.

while the new variable satisfies the stochastic equation:

$$\begin{aligned} \dot{\rho}_{00}(t) &= -\kappa(t)\rho_{00}(t) \\ &- \rho_{00}(t)\sqrt{\frac{\gamma}{2}}\sum_{e,g}\{\mathbf{d}_{eg}\rho_{ge}(t)\mathbf{f}^\dagger(t) + \mathbf{d}_{ge}\rho_{eg}(t)\mathbf{g}^\dagger(t)\}. \end{aligned} \quad (30)$$

In our simulations, we have used a Gaussian pump profile. The stochastic averages are depicted in Fig. 6. For the case of $N = 10$, we encounter the same issue as in Fig. 5, where the steady states are captured incorrectly. For a larger number of atoms ($N = 100$), the situation does not improve, in contrast to Fig. 5 (g, i). Perhaps, the continuous pumping process generates a more intricate steady state, posing challenges for accurate reproduction by our stochastic formalism.

As pointed out in Ref. [28], additional dissipation channels disrupt the formation of the steady states. Ref. [28] assumed the Meitner-Auger decay of the excited state. Alternatively, one could consider non-radiative dissipation to the ground state ($2 \rightarrow 1$) with a rate Γ as follows:

$$\begin{aligned} \dot{\rho}_{11}(t) &= \dots + \Gamma\rho_{22}(t), & \dot{\rho}_{22}(t) &= \dots - \Gamma\rho_{22}(t), \\ \dot{\rho}_{12}(t) &= \dots - \frac{\Gamma}{2}\rho_{12}(t), & \dot{\rho}_{21}(t) &= \dots - \frac{\Gamma}{2}\rho_{21}(t). \end{aligned}$$

As shown in Fig. 7, we have found a minimal value of Γ required to mitigate the discrepancies in Fig. 6. For both

cases of $N = 10$ and $N = 100$, the additional dissipation with the rate of the same order of magnitude as spontaneous emission, i.e., $\Gamma \sim \gamma$, is sufficient for regularization. Based on our experience, systems with a larger number of atoms may require a higher dissipation rate.

In conclusion, the ratio between timescales of superradiance, pumping, and dissipation directly influences the formation of steady states. Notably, when these steady states are less prominent, the stochastic formalism consistently yields accurate averages.

C. Quantum beats in V -system

So far, we have considered only models with lasing between two levels. To demonstrate that our formalism correctly captures many-level effects, we consider a V -type configuration with two excited states $|2\rangle, |3\rangle$ and a single ground state $|1\rangle$, as shown in Fig. 8 (a). The energy gap between excited states Δ is much smaller than the center frequency $\Delta \ll \omega_0$. Fluorescence from emitters with such a level structure may exhibit quantum beating, a fundamental quantum phenomenon that has been observed in various spectral ranges, including optical [61, 62], XUV [63, 64], and X-rays [65]. In the context of collective emission, quantum beating is superimposed with superfluorescent behavior [66, 67]. Here, we consider superfluorescence in Helium gas under presence of

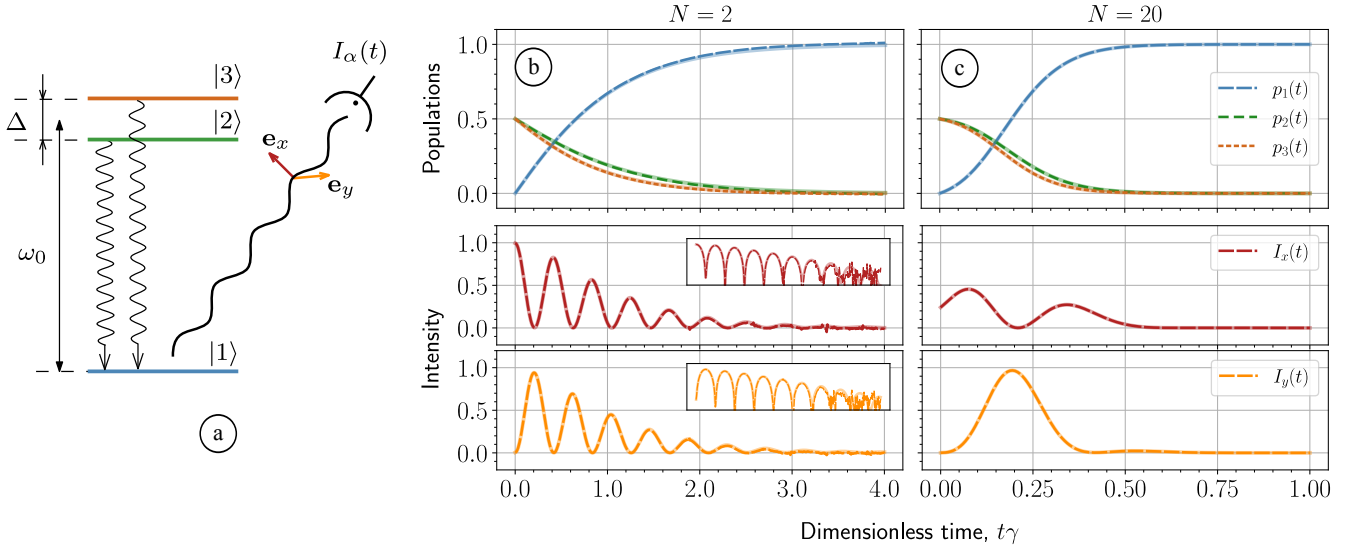


FIG. 8. Quantum beats in a V-type system, depicted on the left (a), calculated for $N = 2$ (b) and $N = 20$ (c) atoms. In both cases, we have taken $\Delta = 15\gamma$, and plotted populations (upper row) and normalized intensities of the field for both polarizations. For $N = 2$ intensity curves (b), we give the same plots in a logarithmic scale in a small box. The intensities of different polarization components are normalized to the maximum full intensity. The semi-transparent lines correspond to quantum expectation values, while the opaque lines represent stochastic averages. In total, the statistical sample contains 10^5 trajectories, with 75 diverging trajectories omitted for the case of $N = 2$ (b).

a weak magnetic field, as in Ref. [64]. We consider transitions from states 2 to 1 and 3 to 1 with slightly different strengths

$$\mathbf{d}_{31} = \frac{d_{31}}{\sqrt{2}}(-\mathbf{e}_x + i\mathbf{e}_y), \quad \mathbf{d}_{21} = \frac{d_{21}}{\sqrt{2}}(\mathbf{e}_x + i\mathbf{e}_y),$$

where $|d_{31}|^2 = 1$ and $|d_{21}|^2 = 0.75$. The transition between the excited states is forbidden, namely $\mathbf{d}_{32} = 0$. If we assume that each atom in the ensemble is initially prepared in a coherent superposition of excited states, such as:

$$|\psi\rangle_a = \frac{|2\rangle_a - |3\rangle_a}{\sqrt{2}},$$

we can observe quantum beats in the intensity of both the x - and y -components of the field [68]. In this scenario, the initial collective state of the ensemble is separable, following Eq. (6), and each atom is characterized by a single-particle density matrix with the following components:

$$\rho_{22}(0) = \rho_{33}(0) = 0.5, \quad \rho_{23}(0) = \rho_{32}(0) = -0.5,$$

while all other matrix elements are zero.

As demonstrated in Fig. 8 (b, c), our formalism reproduces the quantum beats. For $N = 2$ atoms, we additionally plot intensity curves in the logarithmic scale (a small box at the top right corner). As one can see, low-amplitude oscillations are not reproduced because they are at the level of statistical fluctuations. Moreover, there are convergence problems for small numbers

of atoms, namely population $p_1(t)$ slightly exceeds unit. The difference between stochastic and quantum simulations becomes increasingly noticeable at later time intervals. We attribute this to challenges arising from numerically simulating nonlinear stochastic differential equations, especially when the noise component is as large as the deterministic part. Nevertheless, these convergence issues tend to vanish when dealing with a larger number of atoms, as demonstrated in the case of $N = 20$.

Let us also analyze a system starting from a statistical mixture. We focus on the most challenging scenario where the initial state has no coherences, and the excited states are statistically equally populated:

$$\rho_{22}(0) = \rho_{33}(0) = 0.5, \quad \rho_{23}(0) = \rho_{32}(0) = 0.0.$$

In this case, there are no quantum beats in the intensity, and the ensemble evolves into a nontrivial steady state, which we fail to reproduce accurately with our formalism, as depicted in Fig. 9 (a).

With multi-level atoms, we can construct another observable, namely a three-operator correlator:

$$\begin{aligned} & \langle \rho_{12}(t) \rho_{23}(t) \rho_{31}(t) \rangle \\ &= \frac{(N-3)!}{N!} \sum_{\mu_1 \neq \mu_2 \neq \mu_3} \text{Tr}(\hat{\sigma}_{\mu_1,13} \hat{\sigma}_{\mu_2,32} \hat{\sigma}_{\mu_3,21} \hat{\rho}(t)). \end{aligned}$$

Such correlators are often factorized in semi-classical and approximated approaches [35]. However, when there is no initial coherence, any factorization of this operator results in zero. Hence, it is important to demonstrate how our formalism reproduces such correlators.

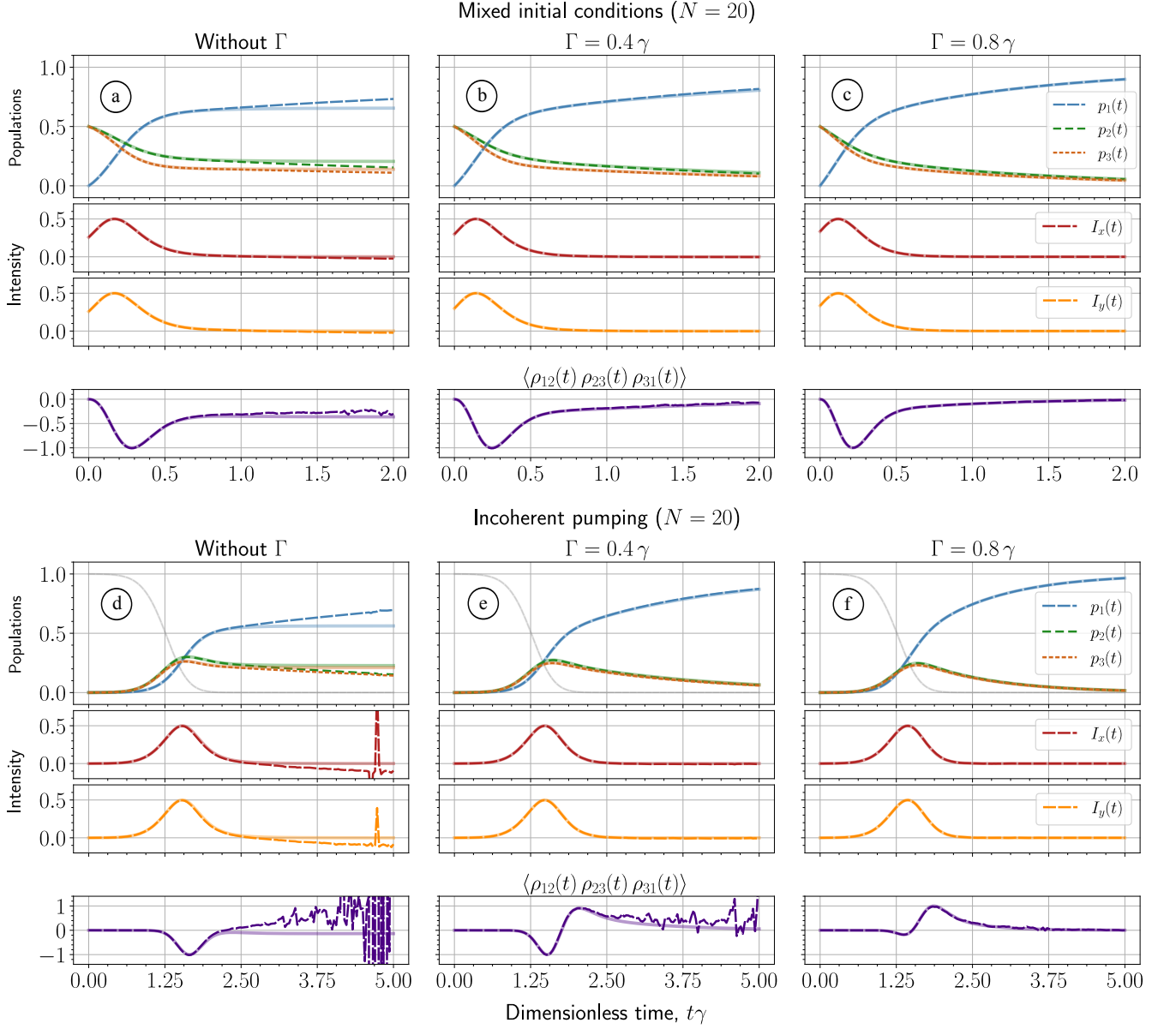


FIG. 9. The dynamics of the ensemble of $N = 20$ atoms with the V-type level structure depicted in Fig. 8 (a). In order to mitigate the discrepancies, we introduce additional non-radiative dissipation channels from the excited states to the ground state ($2, 3 \rightarrow 1$) with a rate Γ (see Eqs. (31)). The semi-transparent lines correspond to quantum expectation values, while the opaque lines represent stochastic averages. In the upper row (a, b, c), atoms start from the mixed state without coherence $\rho_{22}(0) = \rho_{33}(0) = 0.5$, the rest is zero. In the lower row (d, e, f), atoms are incoherently pumped, and similar issues with steady states arise. We chose the same profile as in Fig. 6 for the pump. The gray line demonstrates the evolution of $\rho_{00}(t)$. Overall we averaged over 10^5 trajectories, omitting only 3 trajectories in the case of pumping without additional damping (d).

In reality, the atoms are not pumped instantaneously. To simulate the effect of a pump pulse, we introduce an additional level $|0\rangle$ described by $\rho_{00}(t)$, as in Sec. IV B. All atoms start from this state and are incoherently pumped to the excited states according to:

$$\dot{\rho}_{ee}(t) = \dots + \frac{\kappa(t)}{2} \rho_{00}(t), \quad e = 2, 3,$$

while $\rho_{00}(t)$ satisfies Eq. (30). The simulations in Fig. 9

(d) reveal that the convergence problems are more pronounced when the system is pumped. Specifically, the intensity curves have spikes and the three-operator correlator does not converge after the emission peak around $t\gamma \approx 2.0$. This is due to the stronger influence of steady states since more population is trapped in the excited states compared to the case without pumping.

We regularize these issues by introducing additional non-radiative damping of excited states to the ground

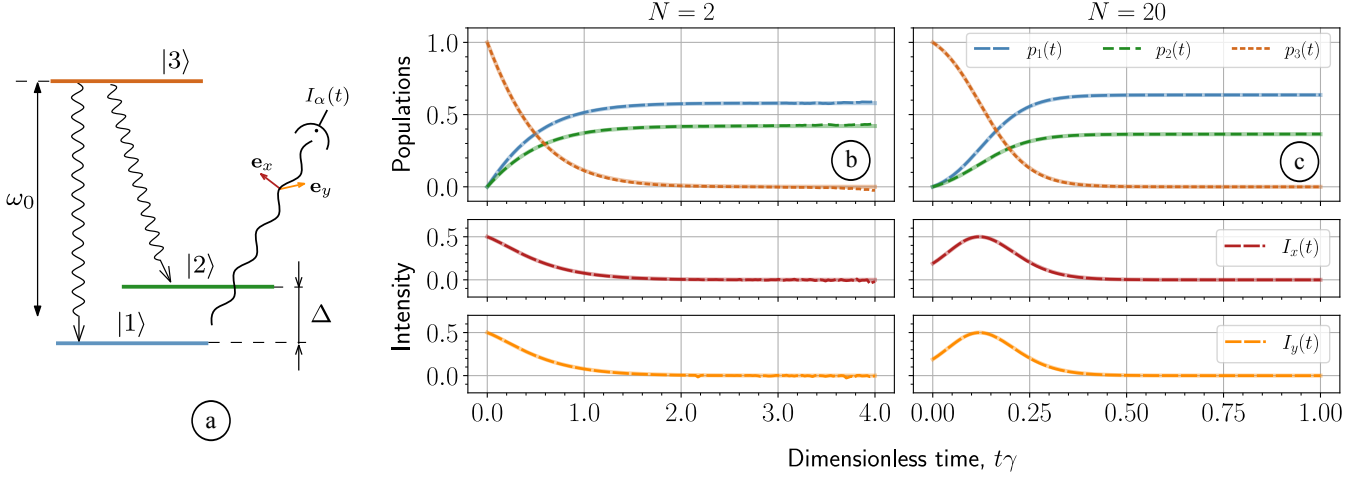


FIG. 10. Lasing from an ensemble of atoms with a Λ -type level structure, as depicted in (a). The separation between ground states Δ is much smaller than the center frequency ω_0 . We present the evolution of populations and intensity components for $N = 2$ (b) and $N = 20$ (c) atoms. Intensity components are normalized to the maximum full intensity. The semi-transparent lines correspond to quantum expectation values, while the opaque lines represent stochastic averages. The statistical sample consists of 10^5 trajectories. For the case of $N = 2$ (b), we have excluded 841 unstable trajectories.

states with a rate Γ :

$$\dot{\rho}_{11}(t) = \dots + \Gamma \sum_e \rho_{ee}(t) \quad (31a)$$

$$\dot{\rho}_{ee}(t) = \dots - \Gamma \rho_{ee}(t), \quad (31b)$$

where $e = 2, 3$. The coherences decay according to:

$$\dot{\rho}_{1e}(t) = \dots - \frac{\Gamma}{2} \rho_{1e}(t), \quad (31c)$$

$$\dot{\rho}_{e1}(t) = \dots - \frac{\Gamma}{2} \rho_{e1}(t), \quad (31d)$$

$$\dot{\rho}_{e_1 e_2}(t) = \dots - \Gamma \rho_{e_1 e_2}(t), \quad (31e)$$

In Fig. 9 (b, c) and (e, f), we have found a minimal value of Γ required to mitigate the discrepancies. As in the previous section, values of $\Gamma \sim \gamma$ are sufficient. With this additional damping, all observables are reproduced accurately for a chosen time range, including the three-operator correlator. This demonstrates that our formalism goes beyond semi-classical models and fully captures the quantum effects of many-body correlations.

D. Lasing in Λ -system

Quantum beats in V -systems are also predicted by semi-classical models or approaches based on stochastic electrodynamics [55]. Nevertheless, certain semi-classical and stochastic models incorrectly predict quantum beats in Λ -systems [55, 69] with one excited $|3\rangle$ and two ground states $|1\rangle, |2\rangle$, which is depicted in Fig. 10 (a). To demonstrate that our formalism has the predictive power of a true quantum model, we study such Λ -configuration with

orthogonal transition polarizations, namely:

$$\mathbf{d}_{31} = \frac{d_{31}}{\sqrt{2}} (-\mathbf{e}_x + i\mathbf{e}_y), \quad \mathbf{d}_{32} = \frac{d_{32}}{\sqrt{2}} (\mathbf{e}_x + i\mathbf{e}_y).$$

Here, $|d_{31}|^2 = 1$ and $|d_{32}|^2 = 0.75$. The transition between the ground states is forbidden.

Our equations predict the absence of intensity beats for any value of Δ , which aligns with the results from quantum simulations. In Fig. 10 (b, c), we present population and intensity curves for $N = 2$ and $N = 20$. Both polarization components of the field share the same profile and do not show any signs of beating. Convergence issues arise in the case of $N = 2$. When the system has reached the ground states, where no dynamics is expected, the population curves exhibit a slight deviation from the quantum expectation values. As previously mentioned, we attribute this discrepancy to the presence of nonlinear noise terms in our equations.

As in the previous section, we also consider the ensemble prepared in a mixed state without coherences. We assume that all levels are initially populated as follows:

$$\rho_{33}(0) = 0.5, \quad \rho_{22}(0) = \rho_{11}(0) = 0.25,$$

and other matrix elements are zero. The solution reveals that the ensemble does not relax completely to the ground states but evolves into a steady state with some population remaining in the excited state, as in Fig. 11 (a). The formation of this state is accompanied by unstable behavior of the three-body correlator, which does not converge after $t\gamma \approx 1.5$.

The same issues appear when the excited state is incoherently pumped with the following additional term in the equations:

$$\rho_{33}(t) = \dots + \kappa(t) \rho_{00}(t),$$

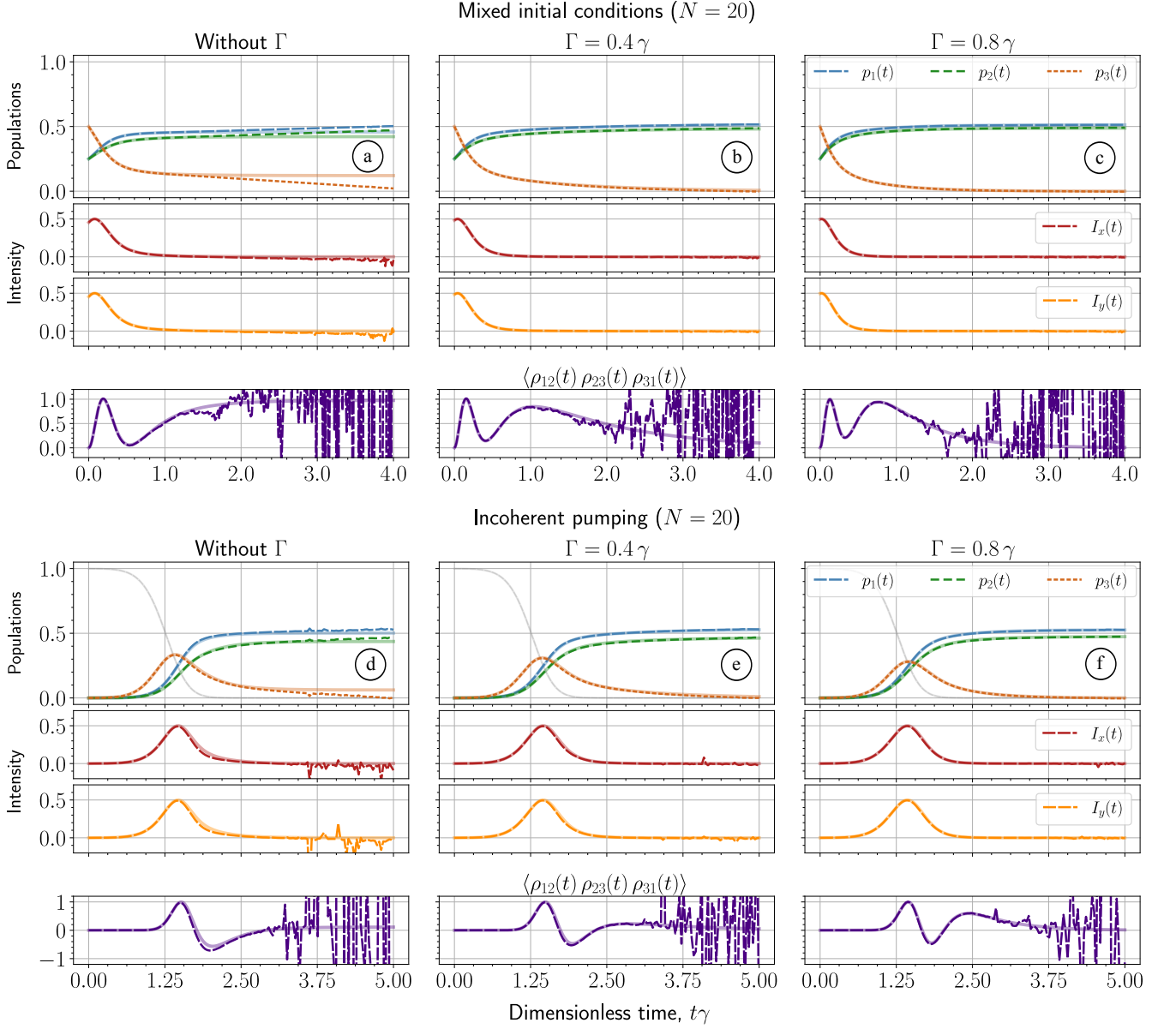


FIG. 11. The dynamics of the ensemble of $N = 20$ atoms with the Λ -type level structure depicted in Fig. 10 (a). The composition of the figure is the same as in Fig. 9. The semi-transparent lines correspond to quantum expectation values, while the opaque lines represent stochastic averages. In the upper row (a, b, c), we consider atoms starting from the mixed initial state $\rho_{11}(0) = \rho_{22}(0) = 0.25$ and $\rho_{33}(0) = 0.50$, rest is zero. In the lower row (d, e, f), atoms are incoherently pumped. To regularize convergence issues, we introduce non-radiative damping of the excited state with a rate Γ (see Eqs. (32)). The gray line demonstrates the evolution of $\rho_{00}(t)$. Overall we averaged over 10^5 trajectories. We have only omitted 9 and 4 trajectories in the case of pumping (a) and mixed initial states (d) without additional damping Γ , respectively.

where $\kappa(t)$ defines the pump profile, and $\rho_{00}(t)$ satisfies Eq. (30). The final state is also a steady state with a nonzero probability of finding an excited atom, as shown in Fig. 11 (d). The stochastic averages converge to incorrect values, and the three-body operator becomes unstable for later time moments.

We attempt to regularize these issues by introducing non-radiative damping of the excited state to the ground

states ($3 \rightarrow 1, 2$) with a rate Γ

$$\dot{\rho}_{33}(t) = \dots - 2\Gamma\rho_{33}(t), \quad (32a)$$

$$\dot{\rho}_{gg}(t) = \dots + \Gamma\rho_{33}(t), \quad (32b)$$

$$\dot{\rho}_{g3}(t) = \dots - \Gamma\rho_{g3}(t), \quad (32c)$$

$$\dot{\rho}_{3g}(t) = \dots - \Gamma\rho_{3g}(t), \quad (32d)$$

where $g = 1, 2$. Consequently, the excited state is depopulated at a rate of 2Γ . We found the damping rates

sufficient to regularize populations and intensities in Fig. 11 (b, c) and (e, f). However, the three-operator correlator still does not converge. The explanation is that the ensemble does not simply evolve into a mixture of ground states. Calculations based on Ref. [28] reveal that the system evolves into a steady state with the following non-zero correlation:

$$\langle \rho_{12}^{(ss)} \rho_{21}^{(ss)} \rangle < 0, \quad (33)$$

where ss stands for steady state. As the product $\rho_{12}^{(ss)} \rho_{21}^{(ss)}$ becomes negative upon averaging, it indicates that the coherences $\rho_{12}(t)$ and $\rho_{21}(t)$ are non-Hermitian at the level of single realizations. This outcome contradicts the intended purpose of our drift gauge, and as a result, our formalism does not accurately reproduce the final state. The coherences between the ground states $\rho_{g_1 \neq g_2}(t)$ are not damped by any additional non-radiative decay, which does not prevent instabilities and slow convergence of the observables involving $\rho_{g_1 \neq g_2}(t)$, such as the analyzed three-particle correlator. Effective regularization would require either stronger decoherence to prevent the buildup of the correlations or the introduction of another dissipation channel for $\rho_{g_1 \neq g_2}(t)$.

V. DISCUSSION

1. Computational effort

First, we address the issue of computational effort. While solving stochastic equations is parallelizable and provides statistically significant results within a few minutes, the complexity of quantum calculations grows polynomially with the number of atoms. For example, in the case of a pumped three-level Λ -configuration (which includes an additional level ρ_{00}), the number of equations grows approximately as $N^7/7!$ [28]. In contrast, the number of stochastic variables is solely determined by the number of atomic levels, as M^2 .

2. High-order correlation functions

Another crucial aspect is the convergence of various expectation values. The higher the order of the correlation function, the more pronounced the challenges with convergence become. This issue is consistently observed when the system reaches a specific steady state, leading to the effective density matrix $\rho_{pq}(t)$ becoming non-Hermitian at the level of individual realizations. This problem was demonstrated in the context of superfluorescence from two-level atoms in Sec. IV A and discussed following Eq. (29). A similar concern was addressed in the context of a Λ -type system after Eq. (33) in Sec. IV D. Since our drift gauge is designed to ensure the Hermitian behavior of the effective density matrix, this issue can only be avoided by introducing additional dissipation

for the problematic steady states. Finding appropriate gauging methods to address these steady states remains an open challenge.

3. Weight function

The last aspect we wish to discuss is related to the drift gauge. In all of our numerical illustrations, the drift gauge is applied only when there is an amplification of emission, specifically when $\text{Re}(\rho_{ee} - \rho_{gg}) \geq 0.0$ for any excited state $|e\rangle$ and ground state $|g\rangle$. In exchange for modifying the equations, we introduce the weight function $\Omega(t)$, which assigns a statistical weight to each trajectory. In principle, the drift gauge can be applied constantly. However, in this case, it turns out that simulations become inaccurate. In contrast, when we use the drift gauge with care, following the guidance provided in Sec. III C, not only our simulations give correct results, but also the contribution of the weight function becomes negligible.

Consider the example of $N = 20$ pumped three-level atoms with a Λ -type level structure, as illustrated in Fig. 10 (a). Similar to the setup in Fig. 11 (f), we introduce non-radiative decay with a rate of $\Gamma = 0.8\gamma$, as in Eqs. (32). In Fig. 11 (f), the statistical averages include the weight function $\Omega(t)$. However, if we apply the drift gauge without using the weight function, the expectation values remain the same, as shown in Fig. 12 (a). The gray-shaded area in the plot illustrates how frequently the drift gauge is applied. As one can observe, the drift gauge is always applied until the intensity reaches its peak. After the peak, the probability of applying the gauge drops abruptly to zero.

In the opposite case, when the drift gauge is constantly applied, the obtained averages are incorrect, both with and without the weight function, as demonstrated in Fig. 12 (b, c). The spiky curves in Fig. 12 (b) represent averages evaluated with the weight function. Since the exponent of the weight function in Eq. (23) depends linearly on the number of atoms N , any relatively large fluctuation becomes strongly amplified, producing sharp spikes. Consequently, our strategy is to apply the drift gauge as rarely as possible. Remarkably, in such cases, the weight function can be omitted.

VI. CONCLUSION

Our primary objective was to establish a numerically efficient and reliable formalism based on first principles to characterize collective spontaneous emission involving any number of multi-level emitters, particularly when incoherent processes are at play.

We focused on compact systems for benchmarking our methodology, as they can be solved exactly through quantum state decomposition. While our methodology

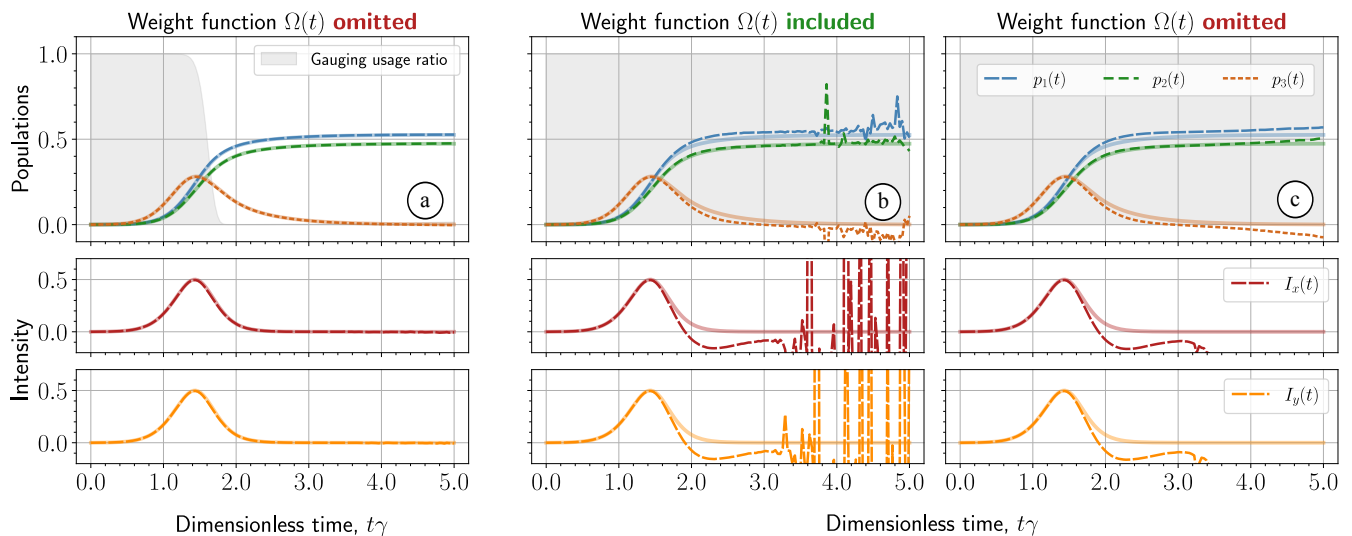


FIG. 12. We revisit the case of $N = 20$ pumped three-level atoms featuring a Λ -type level structure, as illustrated in Fig. 10 (a). Similar to the setup in Fig. 11 (f), we introduce non-radiative decay with a rate of $\Gamma = 0.8\gamma$ (refer to Eqs. (32)). The semi-transparent lines correspond to quantum expectation values, while the opaque lines represent stochastic averages. In the first column (a), we present simulations conducted without the use of the weight function $\Omega(t)$. Nevertheless, the drift gauge is still applied, activated only when population inversions are positive, in accordance with the guidance provided in Sec. III C. The gray-filled area shows how frequently the drift gauge is applied. To provide a comparison, the subsequent two columns (b and c) depict the same simulations with the drift gauge applied constantly, with (b) and without (c) the weight function. Remarkably, not using the weight function results in fewer discrepancies compared to the unnecessary application of the drift gauge.

generally yielded satisfactory results across a wide parameter range, we uncovered discrepancies when the system entered specific steady states. We showed that the presence of incoherent processes mitigated these issues.

Crucially, our formalism is characterized by equations that do not depend on the number of emitters, eliminating the numerical difficulties associated with traditional techniques based on quantum state decomposition.

Throughout the article, we have examined various scenarios and cases, from cooperative emission of instantly excited two-level atoms to complex multi-level systems, such as V - and Λ -type systems, showcasing the versatility and performance of our methodology.

Our work offers valuable insights into the numerical challenges of simulating superfluorescence, the performance and limitations of our methodology, and its practical applicability in studying this fascinating quantum phenomenon.

ACKNOWLEDGMENTS

S.C. and V.S. acknowledge the financial support of Grant-No. HIDSS-0002 DASHH (Data Science in Hamburg-Helmholtz Graduate School for the Structure of the Matter).

[1] R. H. Dicke, Coherence in Spontaneous Radiation Processes, *Phys. Rev.* **93**, 99 (1954).
[2] G. S. Agarwal, Master-Equation Approach to Spontaneous Emission, *Phys. Rev. A* **2**, 2038 (1970).
[3] R. H. Lehberg, Radiation from an N -Atom System. I. General Formalism, *Phys. Rev. A* **2**, 883 (1970).
[4] M. Gross and S. Haroche, Superradiance: An essay on the theory of collective spontaneous emission, *Physics Reports* **93**, 301 (1982).
[5] R. K. Bullough, Photon, quantum and collective, effects from Rydberg atoms in cavities, *Hyperfine Interactions* **37**, 71 (1987).
[6] A. A. Svidzinsky, J.-T. Chang, and M. O. Scully, Cooperative spontaneous emission of N atoms: Many-body

eigenstates, the effect of virtual Lamb shift processes, and analogy with radiation of N classical oscillators, *Phys. Rev. A* **81**, 053821 (2010).
[7] O. Rubies-Bigorda, S. Ostermann, and S. F. Yelin, Characterizing superradiant dynamics in atomic arrays via a cumulant expansion approach, *Phys. Rev. Res.* **5**, 013091 (2023).
[8] N. Skribanowitz, I. P. Herman, J. C. MacGillivray, and M. S. Feld, Observation of Dicke Superradiance in Optically Pumped HF Gas, *Phys. Rev. Lett.* **30**, 309 (1973).
[9] H. M. Gibbs, Q. H. F. Vreken, and H. M. J. Hiksloops, Single-Pulse Superfluorescence in Cesium, *Phys. Rev. Lett.* **39**, 547 (1977).
[10] Q. H. F. Vreken and M. F. H. Schuurmans, Direct Mea-

- surement of the Effective Initial Tipping Angle in Superfluorescence, *Phys. Rev. Lett.* **42**, 224 (1979).
- [11] P. Cahuzac, H. Sontag, and P. Toschek, Visible superfluorescence from atomic europium, *Optics Communications* **31**, 37–41 (1979).
- [12] M. S. Malcuit, J. J. Maki, D. J. Simkin, and R. W. Boyd, Transition from superfluorescence to amplified spontaneous emission, *Phys. Rev. Lett.* **59**, 1189 (1987).
- [13] G. Rainò, M. A. Becker, M. I. Bodnarchuk, R. F. Mahrt, M. V. Kovalenko, and T. Stöferle, Superfluorescence from lead halide perovskite quantum dot superlattices, *Nature* **563**, 671 (2018).
- [14] C. Bradac, M. T. Johnsson, M. van Breugel, B. Q. Baragiola, R. Martin, M. L. Juan, G. K. Brennen, and T. Volz, Room-temperature spontaneous superradiance from single diamond nanocrystals, *Nature Communications* **8**, 10.1038/s41467-017-01397-4 (2017).
- [15] W. Guerin, M. O. Araújo, and R. Kaiser, Subradiance in a Large Cloud of Cold Atoms, *Phys. Rev. Lett.* **116**, 083601 (2016).
- [16] D. C. Gold, P. Huft, C. Young, A. Safari, T. G. Walker, M. Saffman, and D. D. Yavuz, Spatial Coherence of Light in Collective Spontaneous Emission, *PRX Quantum* **3**, 010338 (2022).
- [17] R. Röhlsberger, K. Schlage, B. Sahoo, S. Couet, and R. Ruffer, Collective Lamb Shift in Single-Photon Superradiance, *Science* **328**, 1248 (2010).
- [18] A. Flusberg, T. Mossberg, and S. Hartmann, Observation of Dicke superradiance at $1.30\ \mu\text{m}$ in atomic Tl vapor, *Physics Letters A* **58**, 373–374 (1976).
- [19] M. Gross, C. Fabre, P. Pillet, and S. Haroche, Observation of Near-Infrared Dicke Superradiance on Cascading Transitions in Atomic Sodium, *Physical Review Letters* **36**, 1035–1038 (1976).
- [20] M. Gross, P. Goy, C. Fabre, S. Haroche, and J. M. Raimond, Maser Oscillation and Microwave Superradiance in Small Systems of Rydberg Atoms, *Physical Review Letters* **43**, 343–346 (1979).
- [21] L. Moi, P. Goy, M. Gross, J. M. Raimond, C. Fabre, and S. Haroche, Rydberg-atom masers. I. A theoretical and experimental study of super-radiant systems in the millimeter-wave domain, *Physical Review A* **27**, 2043–2064 (1983).
- [22] N. Rohringer, D. Ryan, R. A. London, M. Purvis, F. Albert, J. Dunn, J. D. Bozek, C. Bostedt, A. Graf, R. Hill, S. P. Hau-Riege, and J. J. Rocca, Atomic inner-shell X-ray laser at 1.46 nanometres pumped by an X-ray free-electron laser, *Nature* **481**, 488 (2012).
- [23] C. Weninger, M. Purvis, D. Ryan, R. A. London, J. D. Bozek, C. Bostedt, A. Graf, G. Brown, J. J. Rocca, and N. Rohringer, Stimulated Electronic X-Ray Raman Scattering, *Phys. Rev. Lett.* **111**, 233902 (2013).
- [24] H. Yoneda, Y. Inubushi, K. Nagamine, Y. Michine, H. Ohashi, H. Yumoto, K. Yamauchi, H. Mimura, H. Kitamura, T. Katayama, T. Ishikawa, and M. Yabashi, Atomic inner-shell laser at 1.5-ångström wavelength pumped by an X-ray free-electron laser, *Nature* **524**, 446 (2015).
- [25] T. Kroll, C. Weninger, R. Alonso-Mori, D. Sokaras, D. Zhu, L. Mercadier, V. P. Majety, A. Marinelli, A. Lutman, M. W. Guetg, F.-J. Decker, S. Boutet, A. Aquila, J. Koglin, J. Koralek, D. P. DePonte, J. Kern, F. D. Fuller, E. Pastor, T. Fransson, Y. Zhang, J. Yano, V. K. Yachandra, N. Rohringer, and U. Bergmann, Stimulated X-Ray Emission Spectroscopy in Transition Metal Complexes, *Phys. Rev. Lett.* **120**, 133203 (2018).
- [26] L. Mercadier, A. Benediktovitch, C. Weninger, M. A. Bleszenohl, S. Bernitt, H. Bekker, S. Dobrodey, A. Sanchez-Gonzalez, B. Erk, C. Bomme, R. Boll, Z. Yin, V. P. Majety, R. Steinbrügge, M. A. Khalal, F. Penent, J. Palaudoux, P. Lablanquie, A. Rudenko, D. Rolles, J. R. Crespo López-Urrutia, and N. Rohringer, Evidence of Extreme Ultraviolet Superfluorescence in Xenon, *Phys. Rev. Lett.* **123**, 023201 (2019).
- [27] R. E. F. Silva and J. Feist, Permutational symmetry for identical multilevel systems: A second-quantized approach, *Physical Review A* **105**, 10.1103/physreva.105.043704 (2022).
- [28] V. Sukharnikov, S. Chuchurka, A. Benediktovitch, and N. Rohringer, Second quantization of open quantum systems in Liouville space, *Physical Review A* **107**, 10.1103/physreva.107.053707 (2023).
- [29] M. Gegg and M. Richter, Efficient and exact numerical approach for many multi-level systems in open system CQED, *New Journal of Physics* **18**, 043037 (2016).
- [30] G. Slavcheva, J. Arnold, and R. Ziolkowski, FDTD Simulation of the Nonlinear Gain Dynamics in Active Optical Waveguides and Semiconductor Microcavities, *IEEE Journal of Selected Topics in Quantum Electronics* **10**, 1052 (2004).
- [31] O. Larroche, D. Ros, A. Klisnick, A. Sureau, C. Möller, and H. Guennou, Maxwell-Bloch modeling of x-ray-laser-signal buildup in single- and double-pass configurations, *Phys. Rev. A* **62**, 043815 (2000).
- [32] H.-T. Chen, T. E. Li, M. Sukharev, A. Nitzan, and J. E. Subotnik, Ehrenfest+R dynamics. I. A mixed quantum-classical electrodynamic simulation of spontaneous emission, *The Journal of Chemical Physics* **150**, 044102 (2019).
- [33] T. E. Li, H.-T. Chen, and J. E. Subotnik, Comparison of Different Classical, Semiclassical, and Quantum Treatments of Light-Matter Interactions: Understanding Energy Conservation, *Journal of Chemical Theory and Computation* **15**, 1957 (2019).
- [34] S. Krušič, K. Bučar, A. Mihelič, and M. Žitnik, Collective effects in the radiative decay of the 2^1P state in helium, *Phys. Rev. A* **98**, 013416 (2018).
- [35] A. Benediktovitch, V. P. Majety, and N. Rohringer, Quantum theory of superfluorescence based on two-point correlation functions, *Physical Review A* **99**, 013839 (2019).
- [36] P. D. Drummond and M. S. Hillery, *The quantum theory of nonlinear optics* (Cambridge University Press, 2014).
- [37] P. Deuar and P. D. Drummond, Stochastic gauges in quantum dynamics for many-body simulations, *Computer Physics Communications* **142**, 442 (2001), arXiv:quant-ph/0203108 [quant-ph].
- [38] S. Wüster, J. F. Corney, J. M. Rost, and P. Deuar, Quantum dynamics of long-range interacting systems using the positive- P and gauge- P representations, *Phys. Rev. E* **96**, 013309 (2017).
- [39] P. Deuar and P. D. Drummond, Correlations in a BEC Collision: First-Principles Quantum Dynamics with 150 000 Atoms, *Phys. Rev. Lett.* **98**, 120402 (2007).
- [40] P. Deuar, A. Ferrier, M. Matuszewski, G. Orso, and M. H. Szymańska, Fully Quantum Scalable Description of Driven-Dissipative Lattice Models, *PRX Quantum* **2**, 010319 (2021).

- [41] A. Gilchrist, C. W. Gardiner, and P. D. Drummond, Positive P representation: Application and validity, *Phys. Rev. A* **55**, 3014 (1997).
- [42] P. Deuar and P. D. Drummond, First-principles quantum dynamics in interacting Bose gases II: stochastic gauges, *Journal of Physics A: Mathematical and General* **39**, 2723 (2006).
- [43] P. Deuar, First-principles quantum simulations of many-mode open interacting Bose gases using stochastic gauge methods, arXiv:cond-mat/0507023 (2005), arXiv: cond-mat/0507023.
- [44] S. Chuchurka, A. Benediktovitch, v. Krušič, A. Halavanau, and N. Rohringer, Stochastic modeling of x-ray superfluorescence (2023).
- [45] R. Friedberg and S. R. Hartmann, Temporal evolution of superradiance in a small sphere, *Physical Review A* **10**, 1728 (1974).
- [46] J. P. Clemens, L. Horvath, B. C. Sanders, and H. J. Carmichael, Collective spontaneous emission from a line of atoms, *Physical Review A* **68**, 023809 (2003).
- [47] R. T. Sutherland and F. Robicheaux, Collective dipole-dipole interactions in an atomic array, *Physical Review A* **94**, 013847 (2016).
- [48] D. Comparat and P. Pillet, Dipole blockade in a cold Rydberg atomic sample, *Journal of the Optical Society of America B* **27**, A208 (2010).
- [49] S. J. Masson and A. Asenjo-Garcia, Universality of Dicke superradiance in arrays of quantum emitters, *Nature Communications* **13**, 2285 (2022).
- [50] E. Sierra, S. J. Masson, and A. Asenjo-Garcia, Dicke Superradiance in Ordered Lattices: Dimensionality Matters, *Physical Review Research* **4**, 023207 (2022).
- [51] F. Andreoli, M. J. Gullans, A. A. High, A. Browaeys, and D. E. Chang, Maximum Refractive Index of an Atomic Medium, *Physical Review X* **11**, 10.1103/physrevx.11.011026 (2021).
- [52] E. V. Goldstein and P. Meystre, Dipole-dipole interaction in optical cavities, *Physical Review A* **56**, 5135 (1997).
- [53] J. M. Raimond, P. Goy, M. Gross, C. Fabre, and S. Haroche, Statistics of Millimeter-Wave Photons Emitted by a Rydberg-Atom Maser: An Experimental Study of Fluctuations in Single-Mode Superradiance, *Physical Review Letters* **49**, 1924 (1982).
- [54] T. Laske, H. Winter, and A. Hemmerich, Pulse Delay Time Statistics in a Superradiant Laser with Calcium Atoms, *Physical Review Letters* **123**, 10.1103/physrevlett.123.103601 (2019).
- [55] M. O. Scully and M. S. Zubairy, *Quantum optics* (1999).
- [56] J. H. Eberly, N. B. Narozhny, and J. J. Sanchez-Mondragon, Periodic Spontaneous Collapse and Revival in a Simple Quantum Model, *Physical Review Letters* **44**, 1323 (1980).
- [57] P. Meystre and M. Sargent, *Elements of Quantum Optics* (Springer Berlin Heidelberg, 2007).
- [58] M. Gegg, *Identical Emitters, Collective Effects and Dissipation in Quantum Optics* (Technische Universität Berlin, 2017).
- [59] C. Rackauckas and Q. Nie, DifferentialEquations.jl – A Performant and Feature-Rich Ecosystem for Solving Differential Equations in Julia, *Journal of Open Research Software* **5**, 15 (2017).
- [60] C. Weninger and N. Rohringer, Transient-gain photoionization x-ray laser, *Phys. Rev. A* **90**, 063828 (2014).
- [61] E. B. Aleksandrov, Optical measurements of the interference of nondegenerate atomic states, *Soviet Physics Uspekhi* **15**, 436 (1973).
- [62] H. Bitto and J. Robert Huber, Molecular quantum beat spectroscopy, *Optics Communications* **80**, 184 (1990).
- [63] Y. Hikosaka, H. Iwayama, and T. Kaneyasu, Zeeman quantum beats of helium Rydberg states excited by synchrotron radiation, *Journal of Synchrotron Radiation* **27**, 675 (2020).
- [64] A. C. LaForge, A. Benediktovitch, V. Sukharnikov, Š. Krušič, M. Žitnik, M. Debatin, R. W. Falcone, J. D. Asmussen, M. Mudrich, R. Michiels, F. Stienkemeier, L. Badano, C. Callegari, M. D. Fraia, M. Ferianis, L. Giannessi, O. Plekan, K. C. Prince, C. Spezzani, N. Rohringer, and N. Berrah, Time-resolved quantum beats in the fluorescence of helium resonantly excited by XUV radiation, *Journal of Physics B: Atomic, Molecular and Optical Physics* **53**, 244012 (2020).
- [65] E. Gerda, R. Ruffer, R. Hollatz, and J. P. Hannon, Quantum Beats from Nuclei Excited by Synchrotron Radiation, *Physical Review Letters* **57**, 1141 (1986).
- [66] Q. H. F. Vrehen, H. M. J. Hiksloops, and H. M. Gibbs, Quantum Beats in Superfluorescence in Atomic Cesium, *Physical Review Letters* **38**, 764 (1977).
- [67] D. Bartholdtsen and R. H. Rinkleff, Superfluorescent transitions in an external magnetic field, *Zeitschrift fuer Physik D Atoms, Molecules and Clusters* **30**, 265 (1994).
- [68] S. Haroche, Quantum beats and time-resolved fluorescence spectroscopy, in *Topics in Applied Physics* (Springer Berlin Heidelberg, 1976) pp. 253–313.
- [69] J. Gea-Banacloche, M. O. Scully, and M. S. Zubairy, Vacuum Fluctuations and Spontaneous Emission in Quantum Optics, *Physica Scripta* **T21**, 81 (1988).
- [70] R. S. Liptser and A. N. Shiryayev, *Statistics of Random Processes I* (Springer New York, 1977).

Appendix A: Stochastic gauges

In Refs. [42, 43], the derivation of the stochastic gauge transformation was based on the freedom in decomposing the density matrix in terms of projectors constructed from coherent states. On one hand, the projectors are not defined uniquely; on the other hand, these projectors are analytical functions of their arguments, providing even more freedom. All of these observations indicate that the probabilistic interpretation of the density matrix is not unique. Since it is sampled using stochastic equations, the choice of these equations is also not unique. The most natural choice of stochastic equations does not necessarily lead to a stable numerical solution. Stochastic gauges offer the possibility of finding a more stable system of equations.

To apply stochastic gauges to our equations, we introduce stochastic freedom in a broader context. Let's start by investigating an arbitrary system of stochastic differential equations that yield a vector of stochastic processes, denoted as $\mathbf{x}(t)$. The exact form of these equations and their origin may be disregarded in this appendix. Consider the following characteristic function:

$$\chi(\boldsymbol{\lambda}, t) = \left\langle \exp [\boldsymbol{\lambda} \cdot \mathbf{x}(t)] \right\rangle. \quad (\text{A1})$$

Its derivatives provide all the necessary information to calculate any expectation values of interest, namely:

$$\langle f[\mathbf{x}(t)] \rangle = f \left[\frac{\partial}{\partial \boldsymbol{\lambda}} \right] \chi(\boldsymbol{\lambda}, t) \Big|_{\boldsymbol{\lambda}=\mathbf{0}}.$$

Consequently, $\chi(\boldsymbol{\lambda}, t)$ is uniquely defined in the vicinity of $\boldsymbol{\lambda} = \mathbf{0}$, since its derivatives at the point $\boldsymbol{\lambda} = \mathbf{0}$ determine all observables.

Now, consider another system of equations that generates a different vector of stochastic processes, denoted as $\mathbf{x}'(t)$, but yields exactly the same expectation values. The corresponding characteristic functions $\chi'(\boldsymbol{\lambda}, t)$ must be identical to $\chi(\boldsymbol{\lambda}, t)$:

$$\chi(\boldsymbol{\lambda}, t) = \chi'(\boldsymbol{\lambda}, t). \quad (\text{A2})$$

The explicit form of the stochastic trajectories $\mathbf{x}(t)$ or $\mathbf{x}'(t)$ is unknown, and only their stochastic differential equations are provided. Therefore, we cannot immediately construct the corresponding characteristic functions and compare them. We can only proceed in the spirit of mathematical induction. First, we ensure that the initial conditions for $\mathbf{x}'(0)$ lead to the same characteristic function, satisfying Eq. (A2) at $t = 0$. Then, assuming that Eq. (A2) holds for later times t , we guarantee that the temporal derivatives of the characteristic functions are preserved:

$$\frac{\partial}{\partial t} \chi(\boldsymbol{\lambda}, t) = \frac{\partial}{\partial t} \chi'(\boldsymbol{\lambda}, t) \quad (\text{A3})$$

The possibility of having multiple equivalent differential equations arises from the fact that the involved stochastic processes are, generally speaking, complex. In other words, the components of the vectors $\mathbf{x}(t)$ and $\mathbf{x}'(t)$ are, in reality, pairs of independent dynamic variables. However, the construction of expectation values does not involve these variables separately. In Eq. (A1), the derivative with respect to λ cannot extract only the real or imaginary part of $x_i(t)$. This property is the key source of stochastic freedom.

Appendix B: Drift gauge

To provide an example of how the concept of stochastic gauge transformations from Appendix A can be applied, we will derive the so-called drift gauge [43] in the spirit of Girsanov's theorem [70]. In certain cases, stochastic differential equations take the form

$$\frac{d\mathbf{x}(t)}{dt} = \mathbf{A}(\mathbf{x}(t), t) + \boldsymbol{\xi}(\mathbf{x}(t), t)$$

where the drift terms $\mathbf{A}(\mathbf{x}, t)$ can lead to diverging stochastic trajectories. Here, $\boldsymbol{\xi}(\mathbf{x}, t)$ represents Gaussian white noise terms with zero first moments and arbitrary second-order correlators. Unfortunately, neglecting diverging trajectories can result in incorrect expectation

values. To tackle the numerical instability of divergent trajectories, one can opt for different stochastic equations with alternative drift terms. We will denote the new solution as $\mathbf{x}'(t)$ and the alternative drift term as $\mathbf{A}'(\mathbf{x}', t)$. The new stochastic differential equations have the same initial conditions and read as follows:

$$\frac{d\mathbf{x}'(t)}{dt} = \mathbf{A}'(\mathbf{x}', t) + \boldsymbol{\xi}(\mathbf{x}'(t), t)$$

To compensate for this change, one can introduce a weight coefficient $\Omega(t) = e^{C_0(t)}$, which can be used to calculate expectation values based on the new stochastic variables:

$$\langle f(\mathbf{x}(t)) \rangle = \langle f(\mathbf{x}'(t)) \Omega(t) \rangle.$$

Consequently, the new characteristic function has the following form:

$$\chi'(\boldsymbol{\lambda}, t) = \left\langle \exp(\boldsymbol{\lambda} \cdot \mathbf{x}'(t) + C_0(t)) \right\rangle.$$

We can always formally write an equation of motion for $C_0(t)$:

$$\frac{dC_0(t)}{dt} = A_0(\mathbf{x}'(t), t) + \xi_0(\mathbf{x}'(t), t),$$

where A_0 is a new drift and ξ_0 is a new Gaussian white noise term. We assume that $\xi_0(\mathbf{x}, t)$ has a zero average and yet unknown correlation properties:

$$\begin{aligned} \langle \xi_0(\mathbf{x}, t) \xi_0(\mathbf{x}, t') \rangle &= \sigma_0(\mathbf{x}, t) \delta(t - t'), \\ \langle \boldsymbol{\xi}(\mathbf{x}, t) \xi_0(\mathbf{x}, t') \rangle &= \boldsymbol{\sigma}(\mathbf{x}, t) \delta(t - t'). \end{aligned}$$

The main goal is to find the drift A_0 for the weight coefficient and the correlation properties σ_0 and $\boldsymbol{\sigma}$ that compensate for the change in drift terms $\Delta \mathbf{A} = \mathbf{A}' - \mathbf{A}$ at the level of the characteristic function. Following Appendix A, we proceed in the spirit of mathematical induction and assume that $\chi'(\boldsymbol{\lambda}, t) = \chi(\boldsymbol{\lambda}, t)$ is satisfied for a certain t . Let's check if the same holds for the derivatives:

$$\begin{aligned} &\frac{\partial}{\partial t} [\chi'(\boldsymbol{\lambda}, t) - \chi(\boldsymbol{\lambda}, t)] \\ &= \left(\boldsymbol{\lambda} \cdot \left[\Delta \mathbf{A} \left(\frac{\partial}{\partial \boldsymbol{\lambda}}, t \right) + \boldsymbol{\sigma} \left(\frac{\partial}{\partial \boldsymbol{\lambda}}, t \right) \right] \right. \\ &\quad \left. A_0 \left(\frac{\partial}{\partial \boldsymbol{\lambda}}, t \right) + \frac{1}{2} \sigma_0 \left(\frac{\partial}{\partial \boldsymbol{\lambda}}, t \right) \right) \chi(\boldsymbol{\lambda}, t). \end{aligned}$$

In the derivation of this expression, we have used Itô's lemma from Eq. (16). To make the right-hand side equal to zero for any $\boldsymbol{\lambda}$, we have to choose the following correlation properties for the noise terms:

$$\begin{aligned} \langle \xi_0(\mathbf{x}, t) \xi_0(\mathbf{x}, t') \rangle &= -2A_0(\mathbf{x}, t) \delta(t - t'), \\ \langle \boldsymbol{\xi}(\mathbf{x}, t) \xi_0(\mathbf{x}, t') \rangle &= -\Delta \mathbf{A}(\mathbf{x}, t) \delta(t - t'). \end{aligned}$$

This constitutes the essence of the drift gauge. Notably, our derivations are not based on the properties of projectors used to decompose the density matrix; our result is applicable to any system of stochastic trajectories, including the modified Bloch equations for the variables $\rho_{pq}(t)$.

Appendix C: Diffusion gauge

In this section, we provide the expressions for $\eta_\alpha(t)$ and $\theta_\alpha(t)$ used in our numerical simulations. These expressions are derived by substituting the decomposition from Eq. (25) into the expression in Eq. (26). Subsequently, we minimize this expression with respect to $\eta_\alpha(t)$ and $\theta_\alpha(t)$, aiming to mitigate the amplification of non-Hermitian components. The resulting functions, $\eta_\alpha(t)$ and $\theta_\alpha(t)$, take the following form:

$$\eta_\beta^4(t) = \frac{\sum_\alpha \left(\left| P_{\alpha\beta}^{(ee)}(t) - P_\alpha^{(+)}(t)P_\beta^{(-)}(t) \right|^2 + \left| P_{\alpha\beta}^{(ge)}(t) - P_\alpha^{(-)}(t)P_\beta^{(-)}(t) \right|^2 \right)}{\sum_\alpha \left(\left| P_{\beta\alpha}^{(eg)}(t) - P_{\alpha\beta}^{(eg)}(t) \right|^2 + \left| P_{\beta\alpha}^{(ee)}(t) - P_{\alpha\beta}^{(gg)}(t) \right|^2 \right)},$$

$$\theta_\beta^4(t) = \frac{\sum_\alpha \left(\left| P_{\beta\alpha}^{(eg)}(t) - P_\alpha^{(+)}(t)P_\beta^{(+)}(t) \right|^2 + \left| P_{\beta\alpha}^{(ee)}(t) - P_\alpha^{(-)}(t)P_\beta^{(+)}(t) \right|^2 \right)}{\sum_\alpha \left(\left| P_{\alpha\beta}^{(ge)}(t) - P_{\beta\alpha}^{(ge)}(t) \right|^2 + \left| P_{\alpha\beta}^{(ee)}(t) - P_{\beta\alpha}^{(gg)}(t) \right|^2 \right)},$$

where for simplicity we introduced the following tensors:

$$P_{\alpha\beta}^{(gg)}(t) = \sum_{e,e',g,g'} d_{eg,\alpha} \rho_{gg'}(t) d_{g'e',\beta},$$

$$P_{\alpha\beta}^{(ge)}(t) = \sum_{e,e',g,g'} d_{eg,\alpha} \rho_{ge'}(t) d_{e'g',\beta},$$

$$P_{\alpha\beta}^{(eg)}(t) = \sum_{e,e',g,g'} d_{ge,\alpha} \rho_{eg'}(t) d_{g'e,\beta},$$

$$P_{\alpha\beta}^{(ee)}(t) = \sum_{e,e',g,g'} d_{ge,\alpha} \rho_{ee'}(t) d_{e'g',\beta},$$

and the following vectors that are stochastic counterparts of the polarization fields:

$$\mathbf{P}^{(+)}(t) = \sum_{e,g} \mathbf{d}_{ge} \rho_{eg}(t),$$

$$\mathbf{P}^{(-)}(t) = \sum_{e,g} \mathbf{d}_{eg} \rho_{ge}(t).$$